Control Engineering Practice 163 (2025) 106395

Contents lists available at ScienceDirect

Control Engineering Practice

journal homepage: www.elsevier.com/locate/conengprac

# A natural indirect adaptive controller for a satellite-mounted manipulator☆

Jacopo Giordano [a,*], Angelo Cenedese [a], Andrea Serrani [b]

[a] Department of Information Engineering, University of Padua, Italy
[b] Department of Electrical, Electronic and Information Engineering "G. Marconi", University of Bologna, Italy

ARTICLE INFO

*Keywords:*
Space robotics and automation
Indirect adaptive control
Nonlinear control

ABSTRACT

The work considers the design of an indirect adaptive controller for a satellite equipped with a robotic arm manipulating an object. Model uncertainty on the manipulated object can considerably impact the overall behavior of the system. In addition, the dynamics of the actuators of the base satellite are non-linear and can be affected by malfunctioning. Neglecting these two phenomena may lead to excessive control effort or to performance degradation. To deal with these issues, an indirect adaptive control approach is pursued in this paper, which allows consideration of relevant features of the actuators' dynamics, such as loss of effectiveness. Furthermore, an adaptive law that preserves the physical consistency of the inertial parameters of the various rigid bodies comprising the system is employed. The performance and robustness of the controller are first analyzed and then validated in a realistic simulation study.

## 1. Introduction

Space operations are in continuous evolution and expansion, both in complexity and reach. In this very dynamic context, satellites equipped with a robotic arm, known as Space Manipulator Systems (SMSs), are envisaged to play pivotal roles across a diverse range of mission scenarios, which can be classified into three main categories: on-orbit servicing (Flores-Abad et al., 2014), active debris removal (Bonnal et al., 2013) and on-orbit assembly and manufacturing (Rognant et al., 2019). Space manipulator systems are characterized by a strong dynamical coupling between the Base Satellite (BS) and the robotic arm, hence necessitating tailored control solutions to achieve the required level of performance (Papadopoulos et al., 2021).

Uncertainties and disturbances could impact considerably the behavior of the SMS. With the exception of the first type of mission, SMS operating in the aforementioned scenarios are particularly susceptible to model uncertainty, which primarily arises from the limited knowledge about the inertial parameters of the target. A further source of uncertainty and disturbance stems from un-modeled nonlinearities in the actuator dynamics, which can be exacerbated by input saturation and component degradation, and may lead to mission failure if not taken into account in the control design. Moreover, it is common practice to neglect the incorporation of orbital dynamics during the design of the control solutions. This omission is justified by the fact that orbital dynamics manifests itself over temporal scales that are considerably longer than those of the manipulation phase. Consequently, such effects are often treated as disturbances.

Two main methodologies can be employed for the design of a controller in the presence of uncertainties and disturbances, namely robust control and adaptive control. In the former, the controller is designed while considering the most severe potential disturbance and uncertainty that could affect the system. In the latter, the parameters of the controller or reference model are tuned to capture uncertainties. In terms of robust control techniques, two particularly popular approaches are $H_\infty$ control and Sliding Mode Control (SMC). In Seddaoui and Saaj (2019) a control solution based on $H_\infty$ control is proposed. However, this control technique in its nonlinear formulation loses many analytical results on robustness and stability established in the linear case. Therefore, in such cases, tuning is generally performed by resorting to trial and error. In Zhao et al. (2019) an SMC controller with an adaptive control gain is designed for SMS systems affected by external disturbance. A robust non-singular terminal SMC is proposed by Shao et al. (2021) to control a SMS and boost the transient performance. The authors of Nicolis et al. (2020) propose a combined SMC and MPC solution where the robustness properties of the first one and the prediction capabilities of the second one are combined. In Dou and Yue (2023) an SMC solution is coupled with a disturbance observer to mitigate the effect of disturbance. All the above-mentioned solutions are robust with respect to the disturbances and unmodeled behaviors; however, they do not attempt to capture the uncertainty related to the partially unknown target and therefore to reduce the resulting regulation effort. A step in this direction has been made by Jia and

☆ This work is partially supported by MUR through PRIN Grant DOCEAT 2020RTWES4 and the Gini Foundation.
* Corresponding author.
*E-mail addresses:* jacopo.giordano@phd.unipd.it (J. Giordano), cenedese@dei.unipd.it (A. Cenedese), andrea.serrani@unibo.it (A. Serrani).

https://doi.org/10.1016/j.conengprac.2025.106395
Received 16 July 2024; Received in revised form 29 April 2025; Accepted 29 April 2025
Available online 16 May 2025
0967-0661/© 2025 The Authors. Published by Elsevier Ltd. This is an open access article under the CC BY license (http://creativecommons.org/licenses/by/4.0/).

Shan (2019) who designed a non-singular terminal SMC controller coupled with a radial basis function neural network for attempting to identify the unmodeled part of the system dynamics. However, the dimensionality of the problem makes this solution viable only for simple robotic arms or single trajectories. Adaptive control has emerged as an effective solution when dealing with model uncertainty that can be adequately captured in a control-oriented model. The uncertainty related to a partial knowledge of the target inertia parameters is amenable to adaptive control strategies, due to regression models that are linear in the uncertain parameters. Within adaptive control theory, two main methods arise: direct and indirect adaptive control. In the direct adaptive approach, the controller parameters are adjusted in real time based on the error system output. In contrast, in the indirect adaptive approach model parameters are adjusted based on an online predictor of the plant model, and the controller gains are updated accordingly. Direct adaptive control offers simplicity, but its lack of modularity may be considered a drawback (Ioannou & Sun, 1996; Krstic et al., 1995). On the other hand, indirect adaptive control offers the possibility of taking into account the actuator dynamics in the adaptive law. Early works along this line for linear systems date back to Annaswamy and Wong (1997) and Karason and Annaswamy (1994). Those features of indirect adaptive control can be exploited for taking into account the effects of actuator saturation and wear directly at the control design level, for example by implementing anti-windup-like mechanisms and adding suitable estimates for losses of actuator efficiency. To date, indirect adaptive control solutions have not been applied to the SMS case yet due to the challenges related to the inversion of the estimated inertia matrix. As a consequence, the totality of the adaptive solutions present in the literature employs direct approaches. An early work adopting adaptive control is Parlaktuna and Ozkan (2004), where a direct adaptive controller for a free-floating SMS based on a direct computed-torque scheme is designed. An inconvenience related to this particular approach is the necessity of acceleration feedback, which is difficult to obtain and possibly corrupted by noise. This problem is avoided in Abiko and Hirzinger (2009) and Wang and Xie (2009), where passivity-based adaptive controllers are proposed. In Wang and Xie (2012) a computed-torque controller in the task space is proposed to deal with kinematic and dynamic uncertainties, acceleration feedback is obtained via an estimator. Other noteworthy approaches are Christidi-Loumpasefski et al. (2020), where a parameter identification method based on angular momentum principles is coupled with a controller, and Yao (2021), where two Neural network-based controllers are considered and actuators saturation are considered explicitly. Nonetheless, the effectiveness of the proposed method depends on restrictive conditions.

Despite a considerable research effort, the problem of dealing with significant model uncertainty, actuator saturation, and reduced actuator effectiveness remains an open problem in SMS applications. One reason is the lack of appropriate extensions of indirect adaptive control schemes, due to the necessity of guaranteeing physical consistency of the estimated inertial parameters for the manipulator and the target. To this end, building on preliminary results presented in Giordano et al. (2024), this paper presents an indirect adaptive control scheme for a free-flying SMS aimed at solving a trajectory tracking problem in the joint space. Inspired by Lee et al. (2018), a *natural adaptation law*, which preserves the underlying Riemannian geometry of inertial parameters, is employed for estimating the inertial parameters of the rigid bodies in the system. This allows an observer-based dynamic estimator to be easily designed, as the resulting estimated inertia matrix is always positive definite, hence invertible. The indirect (hence, predictor-based) nature of the ensuing adaptive controller allows the effect of actuator dynamics and loss of control authority to be incorporated in the updated law, hence alleviating their adversarial effect on parameter estimation when compared to direct adaptive control solutions, as seen in the reported simulation studies.

**Table 1**
Nomenclature.

| Symbol | Definition |
|---|---|
| $\boldsymbol{p}_b^i, \tilde{\boldsymbol{p}}_b^i$ | Position and position error of the BS expressed in $\mathcal{I}$ coordinates |
| $\boldsymbol{R}_b, \tilde{\boldsymbol{R}}_b$ | Rotation matrix from the $\mathcal{B}$ frame to the $\mathcal{I}$ frame and rotation error matrix of the BS |
| $\tilde{\boldsymbol{\sigma}}$ | Orientation error of the BS represented in MRP |
| $\tilde{\boldsymbol{p}}_e^i, \tilde{\boldsymbol{R}}_e$ | Position errors of the EE expressed in $\mathcal{I}$ coordinates and rotation error matrix of the EE |
| $\tilde{\boldsymbol{\sigma}}_e$ | Orientation error of the EE represented in MRP |
| $\boldsymbol{v}_b, \boldsymbol{\omega}_b$ | Linear and angular velocities of the BS with respect to the $\mathcal{I}$ frame expressed in $\mathcal{B}$ coordinates |
| $\boldsymbol{q}$ | Joint variables for the robotic arm. |
| $\dot{\boldsymbol{x}}$ | Generalized velocity |
| $\tilde{\dot{\boldsymbol{x}}}$ | Generalized velocity tracking error |
| $\boldsymbol{f}_b, \boldsymbol{\tau}_b$ | Force and torque applied at the origin of frame $\mathcal{B}$ and expressed in $\mathcal{B}$ coordinates |
| $\boldsymbol{\tau}$ | Torque applied at the robotic arm joints |
| $\boldsymbol{u}$, $\boldsymbol{u}^c$, $\tilde{\boldsymbol{u}}$ | Generalized control forces, generalized commanded control forces, and corresponding deviations |
| $\theta$, $\hat{\theta}$, $\tilde{\theta}$ | Inertia parameters, estimated inertia parameters, and corresponding estimation error |
| $\lambda$, $\hat{\lambda}$, $\tilde{\lambda}$ | Actuators efficiency, estimated actuators efficiency, and corresponding estimation error |
| $\boldsymbol{\xi}$, $\tilde{\boldsymbol{\xi}}$ | Generalized velocity observation and respective observation error |
| $\tilde{\boldsymbol{x}}$ | Combined position and orientation error |
| $\dot{\boldsymbol{x}}_{\text{err}}$, $\hat{\dot{\boldsymbol{x}}}_{\text{err}}$ | Augmented velocity error and its estimate |

The paper is organized as follows: Section 2 sets the notation, whereas in Section 3 the dynamic model of the SMS and its actuators are presented, together with background notions on the space of physically consistent inertial parameters of a rigid body. The design of the adaptive controller is presented in Section 4, together with the ensuing stability analysis. Simulation results are presented and discussed in Section 5. Concluding remarks are offered in Section 6.

## 2. Assumptions and notation

### 2.1. System and environmental assumptions

All the manipulator's joints are supposed to be revolute since prismatic ones are not commonly employed in space. Flexibility of bodies and joints is assumed to be negligible. It is also assumed that the manipulation tasks are performed at a faster time scale than the orbital period, so that the influence of orbital dynamics and gravitational disturbances can be neglected. The SMS is thus modeled as a chain of $n+1$ rigid bodies, arranged from the BS to the end effector (EE). The values of the uncertain inertial parameters of the rigid bodies are assumed to range within known compact sets. Without loss of generality, the grasped object is assumed to be part of the EE.

### 2.2. Notation

The reference frames employed throughout this work are shown in Fig. 1, where $\mathcal{I}$ denotes the inertial frame. For the $j$th rigid body of the kinematic chain, with $j = 0, \dots, n$, a generic body-fixed frame $\mathcal{G}$ is positioned in a geometrically significant pose, and another body-fixed frame $\mathcal{J}$ is placed at its center-of-mass (CoM) and aligned with its principal axes of inertia. Conversely, the frame $\mathcal{G}$ of the BS is placed at its geometric center. For each link of the robotic arm, the frame $\mathcal{G}$ is positioned at the joint center and aligned accordingly to the Denavit–Hartenberg convention. Note that the relative position of the

**Table 2**
List of acronyms.

| Acronym | Description |
|---|---|
| BS | Base Satellite |
| COM | Center of Mass |
| EE | End Effector |
| ISS | Input-to-State Stable (or Stability) |
| MRP | Modified Rodrigues Parameters |
| PWM | Pulse-Width Modulation |
| PWPF | Pulse-Width Pulse-Frequency |
| RCS | Reaction Control System |
| RW | Reaction Wheel |
| SMC | Sliding Mode Control |
| SMS | Space Manipulator System |

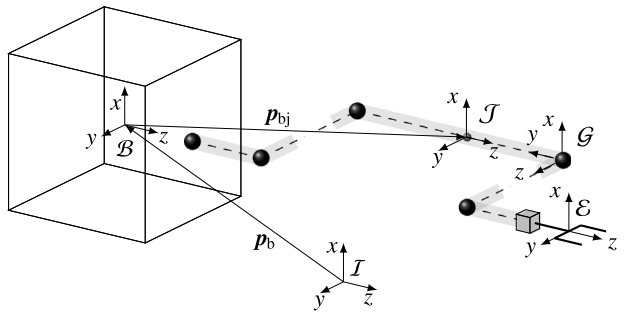


**Fig. 1.** Structure of the SMS with the indication of the frames of interest.

frames $\mathcal{G}$ and $\mathcal{J}$ depends on the location of the center of mass of the corresponding body, hence is affected by model uncertainty. A body frame $\mathcal{B}$ aligned with the $j = 0$ frame $\mathcal{G}$ and a frame $\mathcal{E}$ specifying the EE pose are defined for convenience.

Given three generic frames $\mathcal{M}$, $\mathcal{N}$ and $\mathcal{O}$, the vector $\boldsymbol{p}^o_{mn} \in \mathbb{R}^3$ represents the position of the origin of frame $\mathcal{N}$ relative to the origin of $\mathcal{M}$ expressed in $\mathcal{O}$. Similarly, the linear and angular velocities of $\mathcal{N}$ relative to $\mathcal{M}$ resolved in $\mathcal{O}$ are denoted with $\boldsymbol{v}^o_{mn} \in \mathbb{R}^3$ and $\boldsymbol{\omega}^o_{mn} \in \mathbb{R}^3$, respectively. The rotation matrix needed to align $\mathcal{N}$ with $\mathcal{M}$ is represented with the symbol $\boldsymbol{R}_{mn} \in SO(3)$. The vectors $\boldsymbol{f}^o_m \in \mathbb{R}^3$ and $\boldsymbol{\tau}^o_m \in \mathbb{R}^3$ represent forces and torques applied at the origin of frame $\mathcal{M}$ and expressed in $\mathcal{O}$. The mass and inertia matrix of the $j$th rigid body expressed in frame $\mathcal{O}$ are denoted by the symbols $m_j$ and $\boldsymbol{I}^o_j \in \mathbb{R}^{3\times3}$, respectively. The body frame is used whenever the superscript representing the reference frame is not specified. If a subscript is not specified, then the first frame is replaced by the inertial one. The $n \times n$ identity matrix and zero matrix are respectively denoted by $\mathbb{I}_{n\times n}$ and $\mathbb{0}_{n\times n}$. The Euclidean norm on $\mathbb{R}^n$ is denoted by $|\boldsymbol{x}| = \sqrt{\boldsymbol{x}^T\boldsymbol{x}}$, $\boldsymbol{x} \in \mathbb{R}^n$, whereas the matrix 2-norm is denoted by $||\cdot||$ and the Frobenius norm is denoted by $||\cdot||_F$. Finally, the infinity and asymptotic norms of a signal are defined as follows

$$||\boldsymbol{x}(\cdot)||_\infty := \sup_{t\geq0} |\boldsymbol{x}(t)|, \qquad ||\boldsymbol{x}(\cdot)||_a := \limsup_{t\to\infty} |\boldsymbol{x}(t)|$$

where $\boldsymbol{x}(\cdot)$ is a locally bounded signal (that is, bounded in each closed interval $t \in [t_1, t_2] \subset \mathbb{R}$). For a generic actuator with dynamic model written in the form

$$\dot{x}_{\text{act}} = F_{\text{act}}(x_{\text{act}}, u^c), \qquad u = H_{\text{act}}(x_{\text{act}}, u^c),$$

we denote with the symbol $c$ the *commanded control signal* (that is, the signal $u^c(\cdot)$ computed by the control algorithm) to differentiate it from the actual control action $u(\cdot)$ generated by the actuator. Frequently used symbols are reported in Table 1, whereas a list of acronyms is found in Table 2.

## 3. System dynamics

The dynamical model of the system expressed in body-frame coordinates does not depend on the position and orientation of the BS (Giordano et al., 2019). Using a matrix formulation, the equations of the dynamical model can be written as follows:

$$\boldsymbol{M}(\boldsymbol{q})\ddot{\boldsymbol{x}} + \boldsymbol{C}(\boldsymbol{q}, \dot{\boldsymbol{x}})\dot{\boldsymbol{x}} = \boldsymbol{u} \tag{1}$$

where $\boldsymbol{q} \in \mathbb{R}^n$ are the joint variables, $\boldsymbol{M}(\boldsymbol{q}) \in \mathbb{R}^{(6+n)\times(6+n)}$ is the inertia matrix, $\boldsymbol{C}(\boldsymbol{q}, \dot{\boldsymbol{x}}) \in \mathbb{R}^{(6+n)\times(6+n)}$ is the centrifugal/Coriolis matrix, $\dot{\boldsymbol{x}}^T := \left[\boldsymbol{v}_b^T, \boldsymbol{\omega}_b^T, \dot{\boldsymbol{q}}^T\right]^T \in \mathbb{R}^{6+n}$ and $\boldsymbol{u}^T := \left[\boldsymbol{f}_b^T, \boldsymbol{\tau}_b^T, \boldsymbol{\tau}^T\right]^T \in \mathbb{R}^{6+n}$ are the generalized velocities and forces respectively, with $\boldsymbol{\tau} \in \mathbb{R}^n$ being the torques applied at the arm joints. In greater detail, the inertia matrix can be partitioned into blocks corresponding to the above choice of generalized velocities

$$\boldsymbol{M}(\boldsymbol{q}) = \begin{bmatrix} \boldsymbol{M}_t & \boldsymbol{M}_{tr} & \boldsymbol{M}_{tm} \\ \boldsymbol{M}_{tr}^T & \boldsymbol{M}_r & \boldsymbol{M}_{rm} \\ \boldsymbol{M}_{tm}^T & \boldsymbol{M}_{rm}^T & \boldsymbol{M}_m \end{bmatrix}$$

where

$$\boldsymbol{M}_t = \sum_{j=0}^{n} m_j \mathbb{I}_{3\times3} \in \mathbb{R}^{3\times3}$$

$$\boldsymbol{M}_{tr} = \sum_{j=0}^{n} -[\boldsymbol{p}_{bj}]_\times m_j \in \mathbb{R}^{3\times3}$$

$$\boldsymbol{M}_{tm} = \sum_{j=1}^{n} m_i \boldsymbol{J}_{\boldsymbol{v}_j} \in \mathbb{R}^{3\times n}$$

$$\boldsymbol{M}_r = \boldsymbol{I}_b + \sum_{j=1}^{n} \left(\boldsymbol{I}_j - m_j[\boldsymbol{p}_{bj}]_\times[\boldsymbol{p}_{bj}]_\times\right) \in \mathbb{R}^{3\times3}$$

$$\boldsymbol{M}_{rm} = \sum_{j=1}^{n} \left(\boldsymbol{I}_j \boldsymbol{J}_{\boldsymbol{\omega}_j} + m_j[\boldsymbol{p}_{bj}]_\times \boldsymbol{J}_{\boldsymbol{v}_j}\right) \in \mathbb{R}^{3\times n}$$

$$\boldsymbol{M}_m = \sum_{j=1}^{n} \left(\boldsymbol{J}_{\boldsymbol{\omega}_j}^T \boldsymbol{I}_j \boldsymbol{J}_{\boldsymbol{\omega}_j} + m_j \boldsymbol{J}_{\boldsymbol{v}_j}^T \boldsymbol{J}_{\boldsymbol{v}_j}\right) \in \mathbb{R}^{n\times n}$$

and $\boldsymbol{J}_{\boldsymbol{v}_j}(\boldsymbol{q}) \in \mathbb{R}^{3\times n}$ and $\boldsymbol{J}_{\boldsymbol{\omega}_j}(\boldsymbol{q}) \in \mathbb{R}^{3\times n}$ are the linear and angular velocity Jacobians of the manipulator, respectively, and $[\cdot]_\times \in \mathbb{R}^{3\times3}$ is the skew-symmetric matrix operator. Due to the complexity of their expressions, we omit to report the explicit formulations of each block of the Coriolis matrix $\boldsymbol{C}(\boldsymbol{q}, \dot{\boldsymbol{x}})$. The procedure for computing the entries of the Coriolis matrix is standard, and can be found, for example, in Spong et al. (2020).

### 3.1. Linear formulation with respect to inertial parameters

It is well known that the model (1) admits a linear parameterization with respect to the inertial parameters of the form

$$\boldsymbol{M}(\boldsymbol{q}, \boldsymbol{\theta})\ddot{\boldsymbol{x}} + \boldsymbol{C}(\boldsymbol{q}, \dot{\boldsymbol{x}}, \boldsymbol{\theta})\dot{\boldsymbol{x}} = \boldsymbol{Y}(\boldsymbol{q}, \dot{\boldsymbol{x}}, \ddot{\boldsymbol{x}})\boldsymbol{\theta} \tag{2}$$

where $\boldsymbol{\theta} = \left[\boldsymbol{\theta}_0^T, \ldots, \boldsymbol{\theta}_n^T\right]^T \in \Theta$ collects the inertia parameters of the $n + 1$ rigid bodies, $\Theta = \Pi_{j=0}^n \Theta_j$, $\Theta_j \subset \mathbb{R}^{10}$ is the cartesian product of $n + 1$ known compact convex sets, and $\boldsymbol{Y}(\boldsymbol{q}, \dot{\boldsymbol{x}}, \ddot{\boldsymbol{x}}) \in \mathbb{R}^{(6+n)\times10(n+1)}$ is a regressor. Furthermore, $\boldsymbol{M}(\boldsymbol{q}, \boldsymbol{\theta})$ is positive definite, hence invertible, if $\boldsymbol{\theta}$ is physically consistent. The $j$th vector of rigid body inertial parameters is given by

$$\boldsymbol{\theta}_j = \left[m_j, \boldsymbol{h}_c^T, I^{xx}, I^{yy}, I^{zz}, I^{xy}, I^{yz}, I^{zx}\right]^T \in \Theta_j$$

where $m_j \in \mathbb{R}$ is the mass of the $j$th body, $\boldsymbol{h}_c := m_j \boldsymbol{p}^g_{gj} \in \mathbb{R}^3$ is the product between $m_j$ and the distance from the $j$th joint to the center of mass of the $j$th link, and $I^{\alpha\beta} \in \mathbb{R}$ are the elements of the inertia matrix $\boldsymbol{I}^g_g \in \mathbb{R}^{3\times3}$.

### 3.2. Actuators model

The actuation devices in an SMS can be divided into two groups, one pertaining to the robotic arm, and the other to the BS. The joints of the robotic arm are actuated by electric motors equipped with gearboxes.

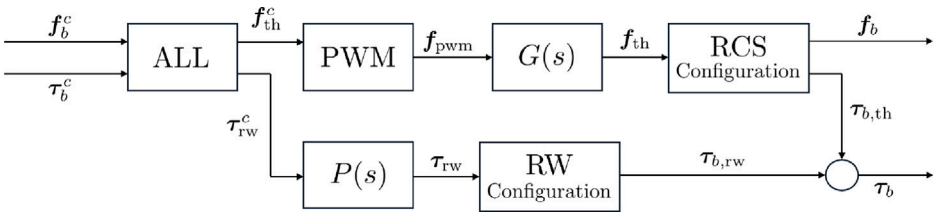


**Fig. 2.** Structure of the actuator system for the base satellite.

As a first approximation, the dynamics of a motor-gearbox assembly can be modeled as a first-order low-pass filter acting element-wise on the components of the commanded torque $\boldsymbol{\tau}^c \in \mathbb{R}^n$. Consequently, the transfer function between the $i$th component of the commanded torque $\boldsymbol{\tau}_c$ and the produced one $\boldsymbol{\tau}$ is given as

$$\tau_i(s) = \frac{\tau_i^c(s)}{T_m s + 1}$$

where $T_m$ is the mechanical time constant of the electric motors, assumed to be the same for each joint. This simplification is justified by the fact that the electrical dynamics of an electric motor are much faster than the mechanical ones. This model of the electric motors captures the primary lag on the commanded torque, obviating the necessity for application-specific information required by a more involved model that explicitly considers the electrical dynamics.

The BS is usually equipped with a Reaction Control System (RCS) and Reaction Wheels (RWs). Force and torque commands for the base satellite, $\boldsymbol{f}_b^c, \boldsymbol{\tau}_b^c \in \mathbb{R}^3$, are mapped onto the set of available actuators by a standard pseudo-inverse based control allocation algorithm, whose description is omitted for reasons of space. As illustrated in Fig. 2, the allocation algorithm generates the vector of thrust commands $\boldsymbol{f}_{\text{th}}^c$ for the RCS and the vector of torque commands for the RW system, $\boldsymbol{\tau}_{\text{rw}}^c$.

A RCS typically consists of a cluster of one-sided jet thrusters, operating in off-on mode. The components of the continuous thrust command $\boldsymbol{f}_{\text{th}}^c$ for each single thruster are modulated by a train of discrete pulses that generates a vector of piece-wise constant commands $\boldsymbol{f}_{\text{pwm}}$ reproducing the desired ones in an averaged sense (e.g., using Pulse Width Modulation (PWM) or Pulse-Width Pulse-Frequency (PWPF)). These discontinuous signals are smoothed by the dynamics of the fuel valves, resulting in the generated thruster forces $\boldsymbol{f}_{\text{th}}$. Without taking into account fluid and combustion dynamics, the behavior of a single jet thruster can be approximated by a second-order low-pass filter simulating the valve transient during opening and closure. The transfer function relating the force commanded by the PWM modulation system and the one produced by the actuator is selected as

$$G(s) = \frac{1}{T_v^2 s^2 + 2T_v s + 1}$$

where $T_v$ is the time constant of the valve. The overall control force and torque produced by the RCS (respectively, $\boldsymbol{f}_b$ and $\boldsymbol{\tau}_{b,\text{th}}$) are related to $\boldsymbol{f}_{\text{th}}$ via a known relation depending only on the thrusters configuration.

A RW system consists of an electric motor controlling a flywheel, producing torque along the axis of rotation. Generally, these wheels are arranged in sets of three or four, and organized to collectively generate torque in any direction within the 3-dimensional Euclidean space. For the same reasons previously outlined for the robotic arm motors, the dynamics of the individual electric motors spinning the flywheel can be approximated using a first-order filter as well, whose transfer function is denoted as $P(s)$ in Fig. 2. If more than one set of RWs is available, the combined torque is found by summing the individual contributions from each RW according to a known geometric configuration. In summary, once the control command $\boldsymbol{u}^c := \left[(\boldsymbol{f}_b^c)^T, (\boldsymbol{\tau}_b^c)^T, (\boldsymbol{\tau}^c)^T\right]^T \in \mathbb{R}^{6+n}$ is assigned by the controller, the generalized control forces $\boldsymbol{u} = \left[\boldsymbol{f}_b^T, \boldsymbol{\tau}_b^T, \boldsymbol{\tau}^T\right]^T \in \mathbb{R}^{6+n}$ produced by the actuators can be computed via known functions that embed all the above-mentioned dynamic effects. Consequently, both the commanded and the actual control signals are available to the designer. While $\boldsymbol{u}(\cdot)$ cannot be directly assigned, it will be employed in the synthesis of the update law of the proposed adaptive controller.

In the sequel, we shall consider performance degradation of individual or multiple actuators, arising from reduced effectiveness or complete loss of control authority. Such effects are modeled at the level of each individual actuator within the architecture presented in this section. However, from the point of view of the model adopted for control design, the overall impact on the control effectiveness will be represented via a modification of the right-hand side of Eq. (2) as follows

$$\boldsymbol{Y}(\boldsymbol{q}, \dot{\boldsymbol{x}}, \ddot{\boldsymbol{x}})\boldsymbol{\theta} = \text{diag}(\boldsymbol{\lambda})\boldsymbol{u} \tag{3}$$

where $\text{diag}(\cdot)$ maps a vector into a diagonal matrix, and $\boldsymbol{\lambda} = \left[\lambda_1, \ldots, \lambda_{6+n}\right]^T$ is an efficiency vector ranging within the convex compact set $\Lambda := \{\boldsymbol{\lambda} \in \mathbb{R}^{6+n} \mid \lambda_{\min} \leq \lambda_i \leq 1,\ \lambda_{\max} \in (0, 1]\}$. While the adopted structure may appear as a somewhat crude lumped-model of otherwise distributed effects, it has been found to be a viable approximation yielding a linear parameterization that is appealing for adaptive control design.

### 3.3. Geometry of the inertial parameters

For physically consistent rigid bodies, the vector $\boldsymbol{\theta}_j$ does not span the entirety of $\mathbb{R}^{10}$ but only a subset of it. As explained in Wensing et al. (2017), the various requirements necessary for physical consistency can be expressed as a single positivity constraint on the symmetric matrix $\boldsymbol{P}_j \in \mathcal{S}(4)$ obtained from $\boldsymbol{\theta}_j$ using the following bijective linear map:

$$f(\boldsymbol{\theta}_j) = \boldsymbol{P}_j = \begin{bmatrix} 0.5\ \text{tr}\left(\boldsymbol{I}_j^j\right)\mathbb{I}_{3\times3} - \boldsymbol{I}_j^j & \boldsymbol{h}_c \\ \boldsymbol{h}_c^T & m \end{bmatrix} \in \mathcal{S}(4) \tag{4}$$

$$f^{-1}(\boldsymbol{P}_j) = \boldsymbol{\theta}_j = \left[m, \boldsymbol{h}_c^T, \text{tr}(\boldsymbol{\Sigma}_j)\,\mathbb{I}_{3\times3} - \boldsymbol{\Sigma}_j\right]^T \in \mathbb{R}^{10}$$

where

$$\boldsymbol{\Sigma}_j = 0.5\text{tr}\left(\boldsymbol{I}_j^j\right)\mathbb{I}_{3\times3} - \boldsymbol{I}_j^j$$

with $\text{tr}(\cdot)$ being the trace operator and $\mathcal{S}(4)$ is set of $4 \times 4$ symmetric matrices. The convex set $\mathcal{M} \subset \mathbb{R}^{10}$ of physically consistent parameters for a rigid body is defined in Lee and Park (2018) as

$$\mathcal{M} = \{\boldsymbol{\theta}_i \in \mathbb{R}^{10} : f(\boldsymbol{\theta}_i) \succ 0\} \simeq \{\boldsymbol{P}_i \in \mathcal{S}(4) : \boldsymbol{P}_i \succ 0\} = \mathcal{P}(4)$$

where $\mathcal{P}(4)$ is the set of $4 \times 4$ symmetric positive definite matrices. When considering the $n + 1$ bodies system as a whole, the set of physically consistent parameters is given by the product space $\mathcal{M}^{n+1} \simeq \mathcal{P}^{n+1}(4)$ which is convex as well. For later use, it is worth defining the set $\mathcal{M}_c = \mathcal{M} \cap \Theta_i$, that is, the set of physically consistent inertial parameters within the compact set $\Theta_i$. As before, when considering $n+1$ rigid bodies, the product space $\mathcal{M}_c^{n+1}$ will be used. The manifold $\mathcal{M}$ inherits the Riemannian structure of $\mathcal{P}(4)$, due to the characteristics of the map $f(\cdot)$ and its inverse. As discussed in Lee and Park (2018), this allows for a coordinate-invariant distance on $\mathcal{M}$ to be defined starting from the affine invariant metric on $\mathcal{P}(4)$. Since $\mathcal{P}(4)$ is an open subset of $\mathcal{S}(4)$, it is possible to define for each $\boldsymbol{P} \in \mathcal{P}(4)$ the set of tangent vectors $T_{\boldsymbol{P}} \in \mathcal{S}(4)$ at $\boldsymbol{P}$. For a point $\boldsymbol{P} \in \mathcal{P}(4)$ and tangent vectors

$\boldsymbol{X}, \boldsymbol{Y} \in T_{\boldsymbol{P}}$, using the above mentioned affine invariant metric it is possible to define the inner product

$$\langle \boldsymbol{X}, \boldsymbol{Y} \rangle_P = \frac{1}{2} \operatorname{tr}(\boldsymbol{P}^{-1}\boldsymbol{X}\boldsymbol{P}^{-1}\boldsymbol{Y})$$

where, again, $\operatorname{tr}(\cdot)$ is the trace operator. This inner product is invariant with respect to the group action $\boldsymbol{Q} * \boldsymbol{P} = \boldsymbol{Q}\boldsymbol{P}\boldsymbol{Q}^T$ with $\boldsymbol{Q} \in GL(4)$, where $GL(4)$ is the set of $4 \times 4$ invertible matrices. The length of a smooth curve $\gamma : \mathbb{R} \to \mathcal{P}(4)$, is defined as follows

$$L(\gamma) = \int_a^b \sqrt{\langle \dot{\gamma}(t), \dot{\gamma}(t) \rangle_{\gamma(t)}}\, dt$$

where $[a, b]$ is a closed interval in $\mathbb{R}$. The distance between two elements $\boldsymbol{P}_1, \boldsymbol{P}_2 \in \mathcal{P}(4)$ is then defined as

$$\begin{aligned} d_{\mathcal{P}(4)}(\boldsymbol{P}_1, \boldsymbol{P}_2) := \inf\{ L(\gamma) \,|\, \gamma : [a, b] \to \mathcal{P}(4), \\ \text{where } \gamma(a) = \boldsymbol{P}_1, \gamma(b) = \boldsymbol{P}_2 \} \end{aligned} \tag{5}$$

It can be shown that the geodesic curve, i.e., the curve that minimizes the distance between two points such that $\gamma_{geo}(0) = \boldsymbol{P}_1$ and $\dot{\gamma}_{geo}(0) = \boldsymbol{V}$ has the following structure

$$\gamma_{geo}(t) = \boldsymbol{P}_1^{\frac{1}{2}} \exp\left( t \boldsymbol{P}_1^{-\frac{1}{2}} \boldsymbol{V} \boldsymbol{P}_1^{-\frac{1}{2}} \right) \boldsymbol{P}_1^{\frac{1}{2}}$$

where $\exp(\cdot)$ is the matrix exponential. In order to ensure that $\gamma_{geo}(1) = \boldsymbol{P}_2$, $\boldsymbol{V}$ must satisfy

$$\boldsymbol{V} = \boldsymbol{P}_1^{\frac{1}{2}} \log\left( \boldsymbol{P}_1^{-\frac{1}{2}} \boldsymbol{P}_2 \boldsymbol{P}_1^{-\frac{1}{2}} \right) \boldsymbol{P}_1^{\frac{1}{2}}$$

which yields the initial velocity at $\boldsymbol{P}_1$ of the unique geodesic connecting $\boldsymbol{P}_1$ and $\boldsymbol{P}_2$. In the above formula, $\log(\cdot)$ denotes the matrix logarithm. It follows that the Riemannian distance between $\boldsymbol{P}_1$ and $\boldsymbol{P}_2$ in $\mathcal{P}(4)$ is given by

$$d_{\mathcal{P}(4)}(\boldsymbol{P}_1, \boldsymbol{P}_2) = || \log\left( \boldsymbol{P}_1^{-1} \boldsymbol{P}_2 \right) ||_F = \left( \sum_{i=1}^{4} \left( \log(\lambda_i) \right)^2 \right)^{\frac{1}{2}}$$

where $\lambda_i$ are the eigenvalues of $\boldsymbol{P}_1^{-1}\boldsymbol{P}_2$ (equivalently, $\boldsymbol{P}_1^{-\frac{1}{2}}\boldsymbol{P}_2\boldsymbol{P}_1^{-\frac{1}{2}}$). At this point, it is possible to construct a distance metric on $\mathcal{M}$ using the map $f(\cdot)$ written in Eq. (4) and the distance in $\mathcal{P}(4)$ defined above:

$$d_{\mathcal{M}}(\boldsymbol{\theta}_1, \boldsymbol{\theta}_2) = d_{\mathcal{P}(4)}(f(\boldsymbol{\theta}_1), f(\boldsymbol{\theta}_2))$$

where $\boldsymbol{\theta}_1, \boldsymbol{\theta}_2 \in \mathcal{M}$. The distance metric so defined possesses several interesting properties, reported in Lee and Park (2018), notably invariance with respect to the choice of coordinate frames, and scale invariance.

### 3.4. Approximation of the distance metric on $\mathcal{M}$

The exact metric distance on $\mathcal{P}(4)$ given in Eq. (5) is not suitable to be used as a Lyapunov function in an adaptive context, due to its nonlinearity. In Lee et al. (2018), a better-suited pseudo-distance metric based on the Bregman divergence of the log-det function $F(\cdot) = -\log(\det(\cdot))$ on $\mathcal{P}(4)$ is proposed for such purpose. Specifically, consider a continuously differentiable, strictly convex function $F : \Omega \to \mathbb{R}$ defined on a convex set $\Omega$. The Bregman divergence associated with $F$ and two points $p, q \in \Omega$, defined as

$$D_{F(\Omega)}(p||q) = F(p) - F(q) - \langle \nabla F(q), p - q \rangle$$

can be interpreted as the difference between the value of $F(\cdot)$ at point $p$ and the value of the first order Taylor expansion $F(\cdot)$ around point $q$ evaluated at $p$. Therefore, if $\Omega = \mathcal{P}(4)$ and $F(\cdot) = -\log(\det(\cdot))$ then the Bregman divergence is given by

$$\begin{aligned} D_{F(\mathcal{P}(4))}(\boldsymbol{P}_2||\boldsymbol{P}_1) &= \log\left( \frac{\det(\boldsymbol{P}_1)}{\det(\boldsymbol{P}_2)} \right) + \operatorname{tr}\left( \boldsymbol{P}_1^{-1}\boldsymbol{P}_2 \right) - 4 \\ &= \log\left( \frac{1}{\prod_{i=1}^{4} \lambda_i} \right) + \sum_{i=1}^{4} \lambda_i - 4 \\ &= \sum_{i=1}^{4} (-\log(\lambda_i) + \lambda_i - 1) \end{aligned}$$

where $\boldsymbol{P}_1, \boldsymbol{P}_2 \in \mathcal{P}(4)$ and the $\lambda_i$ are the eigenvalues of $\boldsymbol{P}_1^{-1}\boldsymbol{P}_2$ (equivalently, $\boldsymbol{P}_1^{-\frac{1}{2}}\boldsymbol{P}_2\boldsymbol{P}_1^{-\frac{1}{2}}$). Being a pseudo-distance, the Bregman divergence fails to be symmetric and to satisfy the triangular inequality, whereas positivity and coordinate invariance are preserved. The two lost properties, however, do not impede the use of this pseudo-distance in the design of adaptive controllers. As a matter of fact, a pseudo-distance metric on $\mathcal{M}$ can be defined using the map $f(\cdot)$ in Eq. (4) together with the Bregman divergence

$$D_{\mathcal{M}}(\boldsymbol{\theta}_1||\boldsymbol{\theta}_2) = D_{F(\mathcal{P}(4))}(f(\boldsymbol{\theta}_2)||f(\boldsymbol{\theta}_1)) \tag{6}$$

It is possible to prove that the pseudo-distance metric $D_{\mathcal{M}}(\boldsymbol{\theta}_1||\boldsymbol{\theta}_2)$ approximates the affine-invariant Riemannian metric $d_{\mathcal{M}}(\boldsymbol{\theta}_1, \boldsymbol{\theta}_2)$ up to second-order (Lee et al., 2018).

## 4. Indirect adaptive controller

In this section, an indirect adaptive controller is designed to achieve asymptotic trajectory tracking for the SMS, despite model parameter uncertainty and loss of actuator efficiency. Estimates of the model's parameters are updated using an adaptive observer, giving rise to a dynamic parameter estimator. The adaptive observer is then used to design the controller. The advantage of using an indirect approach for parameter estimation lies in the modularity of the scheme and advantageous robustness properties in presence of actuator dynamics, whenever these latter are adequately modeled and incorporated in the dynamic estimator. In the context of robotic manipulation, however, the use of an adaptive observer is hindered by the requirement to invert the estimated inertia matrix, which may fail to maintain positive definiteness as the estimated parameters evolve. A projection operator defined on the basis of the pseudo-Riemannian metric thus presented is employed in the update law to ensure consistency of the estimated inertia in the space of positive definite matrices.

### 4.1. Adaptive observer

The adaptive observer, which is used to generate a regressor for both the estimate of the inertial parameters $\hat{\boldsymbol{\theta}}$ and the actuator efficiency $\hat{\boldsymbol{\lambda}}$, is designed as

$$\boldsymbol{M}(\boldsymbol{q}, \hat{\boldsymbol{\theta}})\dot{\boldsymbol{\xi}} = \operatorname{diag}(\hat{\boldsymbol{\lambda}})\boldsymbol{u} - \boldsymbol{C}(\boldsymbol{q}, \dot{\boldsymbol{x}}, \hat{\boldsymbol{\theta}})\boldsymbol{\xi} + \boldsymbol{K}_o(\boldsymbol{q}, \hat{\boldsymbol{\theta}})(\dot{\boldsymbol{x}} - \boldsymbol{\xi}) \tag{7}$$

where $\boldsymbol{\xi} \in \mathbb{R}^{6+n}$ is the observed generalized velocity, $\hat{\boldsymbol{\theta}} \in \mathbb{R}^{10(n+1)}$, $\hat{\boldsymbol{\lambda}} \in \mathbb{R}^{6+n}$, $\boldsymbol{K}_o(\boldsymbol{q}, \hat{\boldsymbol{\theta}}) = k_o \boldsymbol{M}(\boldsymbol{q}, \hat{\boldsymbol{\theta}})$, and $k_o > 0$ is a positive gain. The update laws are selected as

$$\begin{aligned} \dot{\hat{\boldsymbol{\theta}}}_j &= \operatorname*{Proj}_{\hat{\boldsymbol{\theta}}_j \in \Theta_j} \left\{ -\gamma_{\theta_j} g(\hat{\boldsymbol{\theta}}_j)^{-1} \bar{\boldsymbol{Y}}_j^T(\boldsymbol{q}, \dot{\boldsymbol{x}}, \boldsymbol{\xi}, \dot{\boldsymbol{\xi}}) \tilde{\boldsymbol{\xi}} \right\}, \quad j = 1, \dots, n+1 \\ \dot{\hat{\boldsymbol{\lambda}}} &= \operatorname*{Proj}_{\hat{\boldsymbol{\lambda}} \in \Lambda} \left\{ \boldsymbol{\Gamma}_\lambda \operatorname{diag}(\boldsymbol{u}) \tilde{\boldsymbol{\xi}} \right\} \end{aligned} \tag{8}$$

where $\gamma_{\theta_i} \in \mathbb{R}$ is a positive scalar and $\boldsymbol{\Gamma}_\lambda \in \mathbb{R}^{(6+n)\times(6+n)}$ is a symmetric and positive definite gain matrix,

$$\begin{aligned} \bar{\boldsymbol{Y}}(\boldsymbol{q}, \dot{\boldsymbol{x}}, \boldsymbol{\xi}, \dot{\boldsymbol{\xi}})\boldsymbol{\theta} &:= \boldsymbol{M}(\boldsymbol{q}, \boldsymbol{\theta})\dot{\boldsymbol{\xi}} + \boldsymbol{C}(\boldsymbol{q}, \dot{\boldsymbol{x}}, \boldsymbol{\theta})\boldsymbol{\xi} \\ \bar{\boldsymbol{Y}}_j(\boldsymbol{q}, \dot{\boldsymbol{x}}, \boldsymbol{\xi}, \dot{\boldsymbol{\xi}})\boldsymbol{\theta}_j &:= \bar{\boldsymbol{Y}}(\boldsymbol{q}, \dot{\boldsymbol{x}}, \boldsymbol{\xi}, \dot{\boldsymbol{\xi}})\bar{\boldsymbol{\theta}}_j \end{aligned}$$

and $\bar{\boldsymbol{\theta}}_j := \left[ 0, \dots, 0, \boldsymbol{\theta}_j^T, 0, \dots 0 \right]^T \in \mathbb{R}^{10(n+1)}$ has the same structure as that of $\boldsymbol{\theta}$, but with all the entries not related with the $j$th rigid body set to zero. The estimates $\hat{\boldsymbol{\theta}}_j$ and $\hat{\boldsymbol{\lambda}}$ are projected onto the sets $\Theta_j$ and $\Lambda$ defined in Section 3 after Eq. (2) and Eq. (3), respectively. Finally, $\operatorname{Proj}\{\cdot\}$ is the smooth projection operator defined in Krstic et al. (1995), whereas $g(\cdot) \in \mathbb{R}^{10\times10}$ is the pullback of the affine-invariant Riemannian metric on $\mathcal{P}(4)$ to $\mathbb{R}^{10}$ under the mapping $f(\cdot)$

$$[g(\boldsymbol{\phi})]_{i,j} = \operatorname{tr}\left( f(\boldsymbol{\phi})^{-1} f(e_i) f(\boldsymbol{\phi})^{-1} f(e_j) \right) \tag{9}$$

where $e_i, e_j$ are vectors of the canonical basis of $\mathbb{R}^{10}$ (Lee & Park, 2018). It should be noted that, since $\hat{\theta}_j(t)$ is projected into $\Theta_i$, and the use of the pullback $g(\hat{\theta}_j)$ ensures that $\hat{\theta}_j(t) \in \mathcal{M}$, then $\hat{\theta}_j(t) \in \mathcal{M}_c$ for all $t > 0$. Consequently, the matrix $g(\hat{\theta}_j(t))$ is symmetric and positive definite for all $t > 0$.

The following result yields a convenient parameterization of the dynamics of the observation error that is exploited in the forthcoming stability analysis

**Proposition 1.** *Let $\tilde{\xi} := \dot{x} - \xi$, $\tilde{\theta} := \theta - \hat{\theta}$, $\tilde{\lambda} := \lambda - \hat{\lambda}$ be the observation error, the inertial parameter estimates error and the efficiency estimation error, respectively. Given the exogenous signals $\boldsymbol{q}(t)$, $\dot{\boldsymbol{x}}(t)$, $\ddot{\boldsymbol{x}}(t)$, $\boldsymbol{u}(t)$, $t \geq 0$, and the initial conditions $\tilde{\theta}(0)$, $\tilde{\lambda}(0)$, $\tilde{\xi}(0)$, system (7) can be written in the observer error coordinates as follows*

$$\begin{aligned}\boldsymbol{M}(t,\theta)\dot{\tilde{\xi}} + \boldsymbol{C}(t,\theta)\tilde{\xi} = \operatorname{diag}(\tilde{\lambda})\boldsymbol{u}(t) - \boldsymbol{C}(t,\tilde{\theta})\xi \\ - \boldsymbol{M}(t,\tilde{\theta})\left(\ddot{\boldsymbol{x}}(t) - \dot{\tilde{\xi}}\right) - \boldsymbol{K}_{\mathrm{o}}(t,\hat{\theta})\tilde{\xi}\end{aligned} \tag{10}$$

*where the notation*

$$\boldsymbol{M}(t,\cdot) := \boldsymbol{M}\big(\boldsymbol{q}(t),\cdot\big), \quad \boldsymbol{C}(t,\cdot) := \boldsymbol{C}\big(\boldsymbol{q}(t),\dot{\boldsymbol{x}}(t),\cdot\big),$$
$$\boldsymbol{K}(t,\cdot) := \boldsymbol{K}\big(\boldsymbol{q}(t),\cdot\big)$$

*is used to stress the time-varying nature of (10).*

**Proof.** Substituting in (7) the definition of $\tilde{\theta}$ and using the linearity of the model with respect to the inertial parameters, the following relation is obtained

$$\begin{aligned}\boldsymbol{M}(t,\theta)\dot{\xi} = \boldsymbol{M}(t,\tilde{\theta})\dot{\xi} + \operatorname{diag}(\hat{\lambda})\boldsymbol{u} - \boldsymbol{C}(t,\tilde{\theta})\xi \\ + \boldsymbol{C}(t,\theta)\xi + \boldsymbol{K}_{\mathrm{o}}(t,\hat{\theta})\tilde{\xi}\end{aligned} \tag{11}$$

Subtracting (11) from (3) leads to the observation error dynamics written in Eq. (10).

**Proposition 2.** *Assume that the trajectories $\dot{\boldsymbol{x}}(t)$, $\ddot{\boldsymbol{x}}(t)$, $\boldsymbol{q}(t)$, $\boldsymbol{u}(t)$ exist for all $t \geq 0$. Then, all forward trajectories $\tilde{\xi}(t)$, $\tilde{\lambda}(t)$, $\hat{\theta}(t)$ of the observer (7) under the update law (8) exist for all $t \geq 0$ and are bounded. In particular, there exist a constant $\mu_{\tilde{\xi}} > 0$ that depends only on the initial conditions $\tilde{\xi}(0) \in \mathbb{R}^{6+n}$, $\tilde{\lambda}(0) \in \Lambda$, $\hat{\theta}(0) \in \mathcal{M}_c^{n+1}$ such that $|\tilde{\xi}(t)| \leq \mu_{\tilde{\xi}}$ for all $t \geq 0$. Furthermore, if the trajectories $\dot{\boldsymbol{x}}(t)$, $\ddot{\boldsymbol{x}}(t)$, $\boldsymbol{q}(t)$, $\boldsymbol{u}(t)$, $t \geq 0$, are bounded, then*

$$||\tilde{\xi}(\cdot)||_a = 0 \tag{12}$$

**Proof.** Consider the Lyapunov function candidate

$$V(t,\tilde{\xi},\tilde{\lambda},\tilde{\theta}) = V_e(t,\tilde{\xi},\tilde{\lambda}) + V_p(\tilde{\theta}) \tag{13}$$

where the first term

$$V_e(t,\tilde{\xi},\tilde{\lambda}) := \frac{1}{2}\tilde{\xi}^T\boldsymbol{M}(t,\theta)\tilde{\xi} + \frac{1}{2}\tilde{\lambda}^T\boldsymbol{\Gamma}_{\lambda}^{-1}\tilde{\lambda} \tag{14}$$

pertains to the observer and actuators efficiency errors, and

$$V_p(\tilde{\theta}) := \sum_{j=0}^{n}\gamma_{\theta_j}^{-1}D_{F(\mathcal{P}(4))}(f(\hat{\theta}_j)||f(\theta_j)) \tag{15}$$

pertains to the inertial parameter estimates. It is well known that the inertia matrix of an SMS satisfies

$$m_{\min}\mathbb{I}_{(6+n)\times(6+n)} \leq \boldsymbol{M}(\boldsymbol{q},\theta) \leq m_{\max}\mathbb{I}_{(6+n)\times(6+n)} \tag{16}$$

for all $\boldsymbol{q} \in \mathbb{R}^n$ and all $\theta \in \mathcal{M}_c^{n+1}$, where $m_{\min}, m_{\max} > 0$ are the lower and upper bounds of the eigenvalues of the positive definite inertia matrix, respectively. This property, together with the fact that $\boldsymbol{\Gamma}_{\Gamma}^{-1}$ are positive definite constant matrices, imply that $V_e(\cdot)$ is a positive definite, radially unbounded, and decrescent Lyapunov function candidate for the dynamics of $\tilde{\xi}$ and $\tilde{\lambda}$. In Lee et al. (2018), it is also proved that (15) is a suitable Lyapunov function candidate for the estimation error of the inertial parameters (see Appendix A for more details). The Lie derivative of $V_e(t,\tilde{\xi},\tilde{\lambda})$ along the vector field of (10) reads as

$$\begin{aligned}\dot{V}_e &= \tilde{\xi}^T\boldsymbol{M}(t,\theta)\dot{\tilde{\xi}} + \frac{1}{2}\tilde{\xi}^T\dot{\boldsymbol{M}}(t,\theta)\tilde{\xi} + \dot{\tilde{\lambda}}^T\boldsymbol{\Gamma}_{\lambda}^{-1}\tilde{\lambda} \\ &= \tilde{\xi}^T\Big[-\boldsymbol{C}(t,\theta)\tilde{\xi} + \operatorname{diag}(\tilde{\lambda})\boldsymbol{u}(t) - \boldsymbol{C}(t,\tilde{\theta})\xi - \boldsymbol{M}(t,\tilde{\theta})\dot{\xi}(t) \\ &\quad - \boldsymbol{K}_{\mathrm{o}}(t,\hat{\theta})\tilde{\xi}\Big] + \frac{1}{2}\tilde{\xi}^T\dot{\boldsymbol{M}}(t,\theta)\tilde{\xi} + \dot{\tilde{\lambda}}^T\boldsymbol{\Gamma}_{\lambda}^{-1}\tilde{\lambda} \\ &= \tilde{\xi}^T\left[\frac{1}{2}\dot{\boldsymbol{M}}(t,\theta) - \boldsymbol{C}(t,\theta)\right]\tilde{\xi} - \tilde{\xi}^T\boldsymbol{Y}(\boldsymbol{q},\dot{\boldsymbol{x}},\xi,\dot{\xi})\tilde{\theta} \\ &\quad - \tilde{\xi}^T\boldsymbol{K}_{\mathrm{o}}(t,\hat{\theta})\tilde{\xi} + \tilde{\xi}^T\operatorname{diag}(\boldsymbol{u})\tilde{\lambda} + \dot{\tilde{\lambda}}^T\boldsymbol{\Gamma}_{\lambda}^{-1}\tilde{\lambda} \\ &= \tilde{\xi}^T\operatorname{diag}(\boldsymbol{u})\tilde{\lambda} + \dot{\tilde{\lambda}}^T\boldsymbol{\Gamma}_{\lambda}^{-1}\tilde{\lambda} - \tilde{\xi}^T\boldsymbol{Y}(\boldsymbol{q},\dot{\boldsymbol{x}},\xi,\dot{\xi})\tilde{\theta} \\ &\quad - \tilde{\xi}^T\boldsymbol{K}_{\mathrm{o}}(t,\hat{\theta})\tilde{\xi}\end{aligned} \tag{17}$$

where Proposition 1 and the skew symmetry of $\dot{\boldsymbol{M}}(\cdot) - 2\boldsymbol{C}(\cdot)$ have been used. It is recalled the following property of the projection operator (Krstic et al., 1995, Appendix E):

$$\boldsymbol{b}^T\operatorname*{Proj}_{\boldsymbol{a}\in\mathcal{A}}\{\boldsymbol{a}\} \leq -\boldsymbol{b}^T\boldsymbol{a}, \quad \forall\boldsymbol{b} \in \mathbb{R}^n, \forall\boldsymbol{a} \in \mathcal{A} \subseteq \mathbb{R}^n$$

where $\mathcal{A}$ is a convex and compact set. Using this property and substituting the update law of $\dot{\hat{\lambda}}$ in (17) yields

$$\dot{V}_e(t,\tilde{\xi},\tilde{\lambda}) \leq -\tilde{\xi}^T\boldsymbol{K}_{\mathrm{o}}(t,\hat{\theta})\tilde{\xi} - \tilde{\xi}^T\boldsymbol{Y}(\boldsymbol{q},\dot{\boldsymbol{x}},\xi,\dot{\xi})\tilde{\theta} \tag{18}$$

Following Lee et al. (2018), the Lie derivative of $V_p(\tilde{\theta})$ satisfies

$$\dot{V}_p(\tilde{\theta}) = -\sum_{j=0}^{n}\gamma_{\theta_j}^{-1}\dot{\hat{\theta}}_j^T g(\hat{\theta}_j)\tilde{\theta}_j \tag{19}$$

owing to the properties of the pullback operator (9) detailed in Appendix A. Substituting the update law of the inertial parameter estimates in (19), one obtains

$$\dot{V}_p(\tilde{\theta}) = \tilde{\xi}^T\boldsymbol{Y}(\boldsymbol{q},\dot{\boldsymbol{x}},\xi,\dot{\xi})\tilde{\theta} \tag{20}$$

Combining (18) and (20), the Lie derivative of the Lyapunov function (13) is found to satisfy the inequality

$$\dot{V}(t,\tilde{\xi},\tilde{\lambda},\tilde{\rho},\tilde{\theta}) \leq -\tilde{\xi}^T\boldsymbol{K}_{\mathrm{o}}(t,\hat{\theta})\tilde{\xi} \leq 0$$

The above equation implies that for all $\xi(0)$, $\hat{\lambda}(0)$, $\hat{\theta}(0)$, along solutions of (10), the Lyapunov function candidate satisfies

$$V(t,\tilde{\xi}(t),\tilde{\lambda}(t),\tilde{\rho}(t),\tilde{\theta}(t)) \leq V(0,\tilde{\xi}(0),\tilde{\lambda}(0),\tilde{\rho}(0),\tilde{\theta}(0)) \tag{21}$$

for all $t \in [0, T_{\max})$, where $[0, T_{\max})$ is the maximal interval of existence and uniqueness of the solutions of the augmented system (1), (7) and (8). Therefore, there exists $\mu_{\tilde{\xi}} > 0$ such that $|\tilde{\xi}(t)| \leq \mu_{\tilde{\xi}}$ for all $t \in [0, T_{\max})$, and this proves the first statement of the theorem, that is, existence and boundedness of $\tilde{\xi}(t)$, $\tilde{\lambda}(t)$ and $\hat{\theta}(t)$ in case $T_{\max} = +\infty$. Finally, under the hypothesis of boundedness of all signals, application of La Salle/Yoshizawa theorem yields asymptotic convergence of the observation error due to uniform positive definiteness of $\boldsymbol{K}_o(t,\hat{\theta})$ (see (16)).

### 4.2. Adaptive controller

In this subsection, a controller based on the observer dynamics is designed, and convergence of the tracking error is proven when $\tilde{\xi}(t) = 0$. The position and velocity error of the BS with respect to given smooth reference trajectories $(\boldsymbol{p}_{b,\mathrm{ref}}^i(t), \boldsymbol{v}_{b,\mathrm{ref}}(t)) \in \mathbb{R}^3 \times \mathbb{R}^3$, $t \geq 0$, are defined as

$$\tilde{\boldsymbol{p}}_b^i := \boldsymbol{p}_b^i - \boldsymbol{p}_{b,\mathrm{ref}}^i, \quad \tilde{\boldsymbol{v}}_b := \boldsymbol{v}_b - \boldsymbol{v}_{b,\mathrm{ref}} = \boldsymbol{R}_b^T\dot{\tilde{\boldsymbol{p}}}_b^i \tag{22}$$

with orientation and angular velocity errors with respect to smooth reference attitude trajectories $(\boldsymbol{R}_{b,\mathrm{ref}}(t), \boldsymbol{\omega}_{b,\mathrm{ref}}(t)) \in SO(3) \times \mathbb{R}^3$, $t \geq 0$, given by

$$\tilde{\boldsymbol{R}} := \boldsymbol{R}_{b,\mathrm{ref}}^T\boldsymbol{R}_b, \quad \tilde{\boldsymbol{\omega}}_b := \boldsymbol{\omega}_b - \boldsymbol{\omega}_{b,\mathrm{ref}} = \boldsymbol{\omega}_b - \tilde{\boldsymbol{R}}^T\boldsymbol{\omega}_{b,\mathrm{ref}}^{\mathrm{ref}} \tag{23}$$

To avoid manipulating rotation matrices, the orientation error $\tilde{\boldsymbol{R}} \in SO(3)$ is parameterized via its Modified Rodriguez Parameters (MRP),

$\tilde{\boldsymbol{\sigma}} \in \mathbb{R}^3$ (Tsiotras, 1996). Note that $\tilde{\boldsymbol{R}} = \mathbb{I}_{3\times3}$ corresponds to $\tilde{\boldsymbol{\sigma}} = 0$. The propagation equation of the MRP reads as

$$\dot{\tilde{\boldsymbol{\sigma}}} = \frac{1}{2}\boldsymbol{G}(\tilde{\boldsymbol{\sigma}})\tilde{\boldsymbol{\omega}}_b \tag{24}$$

where

$$\boldsymbol{G}(\tilde{\boldsymbol{\sigma}}) := \frac{1+\tilde{\boldsymbol{\sigma}}^T\tilde{\boldsymbol{\sigma}}}{2}\mathbb{I}_{3\times3} + [\tilde{\boldsymbol{\sigma}}]_\times + [\tilde{\boldsymbol{\sigma}}]_\times^2.$$

The position and velocity errors of the joint variables are defined respectively as

$$\tilde{\boldsymbol{q}} := \boldsymbol{q} - \boldsymbol{q}_{\text{ref}} \qquad \dot{\tilde{\boldsymbol{q}}} := \dot{\boldsymbol{q}} - \dot{\boldsymbol{q}}_{\text{ref}} \tag{25}$$

Next, *augmented velocity errors* are defined with the purpose of inducing a stabilizing action on the position, attitude and joint variable error dynamics. Specifically, let the augmented error $\dot{\boldsymbol{x}}_{\text{err}} = [\boldsymbol{\nu}_{\text{err}}^T, \boldsymbol{\omega}_{\text{err}}^T, \dot{\boldsymbol{q}}_{\text{err}}^T]^T \in \mathbb{R}^{6+n}$ be defined as

$$\dot{\boldsymbol{x}}_{\text{err}} := \boldsymbol{K}_{\bar{\text{x}}}(\boldsymbol{R}_b)\bar{\boldsymbol{x}} + \dot{\tilde{\boldsymbol{x}}} \tag{26}$$

where $\bar{\boldsymbol{x}} := [(\tilde{\boldsymbol{p}}_b^i)^T, \tilde{\boldsymbol{\sigma}}^T, \tilde{\boldsymbol{q}}^T]^T \in \mathbb{R}^{(6+n)}$ is the modified position and orientation error, $\dot{\tilde{\boldsymbol{x}}} = [\tilde{\boldsymbol{\nu}}_b^T, \tilde{\boldsymbol{\omega}}_b^T, \dot{\tilde{\boldsymbol{q}}}^T]^T := \dot{\boldsymbol{x}} - \dot{\boldsymbol{x}}_{\text{ref}} \in \mathbb{R}^{(6+n)}$, is the velocity tracking error, and

$$\boldsymbol{K}_{\bar{\text{x}}}(\boldsymbol{R}_{\text{b}}) := \begin{bmatrix} \boldsymbol{R}_b^T\boldsymbol{K}_{\text{p}} & \mathbb{0} & \mathbb{0} \\ \mathbb{0} & \boldsymbol{K}_\sigma & \mathbb{0} \\ \mathbb{0} & \mathbb{0} & \boldsymbol{K}_{\text{q}} \end{bmatrix} \in \mathbb{R}^{(6+n)\times(6+n)}$$

where $\boldsymbol{K}_{\text{p}} \in \mathbb{R}^{3\times3}$, $\boldsymbol{K}_\sigma \in \mathbb{R}^{3\times3}$, $\boldsymbol{K}_{\text{q}} \in \mathbb{R}^{n\times n}$ are positive definite constant gain matrices. In correspondence to (26), the dynamics of the modified position and orientation error, $\bar{\boldsymbol{x}}$, is written component-wise as

$$\begin{aligned} \dot{\tilde{\boldsymbol{p}}}_b^i &= \boldsymbol{R}_b\tilde{\boldsymbol{\nu}}_b = -\boldsymbol{K}_p\tilde{\boldsymbol{p}}_b^i + \boldsymbol{\nu}_{\text{err}} \\ \dot{\tilde{\boldsymbol{\sigma}}} &= \frac{1}{2}\boldsymbol{G}(\tilde{\boldsymbol{\sigma}})\left[-\boldsymbol{K}_\sigma\tilde{\boldsymbol{\sigma}} + \boldsymbol{\omega}_{\text{err}}\right] \\ \dot{\tilde{\boldsymbol{q}}} &= -\boldsymbol{K}_q\tilde{\boldsymbol{q}} + \dot{\boldsymbol{q}}_{\text{err}} \end{aligned} \tag{27}$$

**Proposition 3.**

*Assume that the trajectory $\dot{\boldsymbol{x}}_{\text{err}}(t)$ exists for all $t \geq 0$. Then, the dynamics of the modified position and orientation error (27) is input-to-state stable (ISS) (Sontag, 2008) with respect to the input $\dot{\boldsymbol{x}}_{\text{err}}(\cdot)$. In particular, the bounds*

$$\begin{aligned} ||\tilde{\boldsymbol{p}}_b^i(\cdot)||_\infty &\leq \max\left\{|\tilde{\boldsymbol{p}}_b^i(0)|, \frac{1}{\lambda_{\min}(\boldsymbol{K}_{\text{p}})}||\boldsymbol{\nu}_{\text{err}}(\cdot)||_\infty\right\} \\ ||\tilde{\boldsymbol{\sigma}}(\cdot)||_\infty &\leq \max\left\{|\tilde{\boldsymbol{\sigma}}(0)|, \frac{1}{\lambda_{\min}(\boldsymbol{K}_\sigma)}||\boldsymbol{\omega}_{\text{err}}(\cdot)||_\infty\right\} \\ ||\tilde{\boldsymbol{q}}(\cdot)||_\infty &\leq \max\left\{|\tilde{\boldsymbol{q}}(0)|, \frac{1}{\lambda_{\min}(\boldsymbol{K}_{\text{q}})}||\boldsymbol{q}_{\text{err}}(\cdot)||_\infty\right\} \end{aligned} \tag{28}$$

*and*

$$\begin{aligned} &||\tilde{\boldsymbol{p}}_b^i(\cdot)||_a \leq \frac{1}{\lambda_{\min}(\boldsymbol{K}_{\text{p}})}||\boldsymbol{\nu}_{\text{err}}(\cdot)||_a, \quad ||\tilde{\boldsymbol{\sigma}}(\cdot)||_a \leq \frac{1}{\lambda_{\min}(\boldsymbol{K}_\sigma)}||\boldsymbol{\omega}_{\text{err}}(\cdot)||_a \\ &||\tilde{\boldsymbol{q}}(\cdot)||_a \leq \frac{1}{\lambda_{\min}(\boldsymbol{K}_{\text{q}})}||\boldsymbol{q}_{\text{err}}(\cdot)||_a \end{aligned} \tag{29}$$

*hold, where $\lambda_{\min}(\cdot)$ denotes the minimum eigenvalue of a matrix.*

**Proof.** The result follows immediately from Lemma 3.3 of Teel (1996) applied to the Lyapunov functions $V_1(\tilde{\boldsymbol{p}}_b^i) = \frac{1}{2}\left(\tilde{\boldsymbol{p}}_b^i\right)^T\tilde{\boldsymbol{p}}_b^i$, $V_2(\tilde{\boldsymbol{\sigma}}) = 2\ln(1+\tilde{\boldsymbol{\sigma}}^T\tilde{\boldsymbol{\sigma}})$, and $V_3(\tilde{\boldsymbol{q}}) = \frac{1}{2}\tilde{\boldsymbol{q}}^T\tilde{\boldsymbol{q}}$, respectively. More details on the proof are reported in Appendix B.

The remaining objective is to regulate $\dot{\boldsymbol{x}}_{\text{err}}(t)$ to zero. To this end, consider the time derivative of (26)

$$\ddot{\boldsymbol{x}}_{\text{err}} = \dot{\boldsymbol{K}}_{\bar{\text{x}}}(\boldsymbol{R}_b, \boldsymbol{\omega}_b)\bar{\boldsymbol{x}} + \boldsymbol{K}_{\bar{\text{x}}}(\boldsymbol{R}_b)\dot{\tilde{\boldsymbol{x}}} + \ddot{\tilde{\boldsymbol{x}}} \tag{30}$$

where $\dot{\tilde{\boldsymbol{x}}} \in \mathbb{R}^{6+n}$ and $\dot{\boldsymbol{K}}_{\bar{\text{x}}}(\boldsymbol{R}_b, \boldsymbol{\omega}_b) \in \mathbb{R}^{(6+n)\times(6+n)}$ is defined as

$$\dot{\boldsymbol{K}}_{\bar{\text{x}}}(\boldsymbol{R}_b(t), \boldsymbol{\omega}_b(t)) := \frac{d}{dt}\boldsymbol{K}_{\bar{\text{x}}}(\boldsymbol{R}_b(t)) = \begin{bmatrix} [\boldsymbol{\omega}_b(t)]_\times\boldsymbol{R}_b^T(t)\boldsymbol{K}_{\text{p}} & \mathbb{0} & \mathbb{0} \\ \mathbb{0} & \mathbb{0} & \mathbb{0} \\ \mathbb{0} & \mathbb{0} & \mathbb{0} \end{bmatrix}$$

Substituting $\ddot{\boldsymbol{x}} = \ddot{\tilde{\boldsymbol{x}}} + \ddot{\boldsymbol{x}}_{\text{ref}}$ in (3) and using (30) leads to the following expression of the dynamics of $\dot{\boldsymbol{x}}_{\text{err}}$

$$\begin{aligned} \boldsymbol{M}(t,\boldsymbol{\theta})\ddot{\boldsymbol{x}}_{\text{err}} = \boldsymbol{M}(t,\boldsymbol{\theta})\big(&\boldsymbol{K}_{\bar{\text{x}}}(\boldsymbol{R}_b)\dot{\tilde{\boldsymbol{x}}} + \dot{\boldsymbol{K}}_{\bar{\text{x}}}(\boldsymbol{R}_b, \boldsymbol{\omega}_b)\bar{\boldsymbol{x}}\big) \\ &- \boldsymbol{C}(t,\boldsymbol{\theta})\dot{\boldsymbol{x}} - \boldsymbol{M}(t,\boldsymbol{\theta})\ddot{\boldsymbol{x}}_{\text{ref}} + \text{diag}(\boldsymbol{\lambda})\boldsymbol{u} \end{aligned}$$

It is clear from the above equation that the $\dot{\boldsymbol{x}}_{\text{err}}$ dynamics depends on the unknown parameter $\boldsymbol{\theta}$. To overcome this problem we shall define an estimated version of the augmented velocity error $\dot{\hat{\boldsymbol{x}}}_{\text{err}}$ and control its dynamics, which depends on the adaptive observer (7). To this end, define the *estimated augmented error* $\dot{\hat{\boldsymbol{x}}}_{\text{err}}$ as

$$\dot{\hat{\boldsymbol{x}}}_{\text{err}} := \dot{\boldsymbol{x}}_{\text{err}} - \tilde{\boldsymbol{\xi}}$$

and note that $\dot{\hat{\boldsymbol{x}}}_{\text{err}} = \dot{\boldsymbol{x}}_{\text{err}}$ whenever $\tilde{\boldsymbol{\xi}} = 0$. Recalling the definition of $\tilde{\boldsymbol{\xi}}$ given in Proposition 1, and using Eq. (26), one obtains a similar expression for the estimated augmented velocity error

$$\dot{\hat{\boldsymbol{x}}}_{\text{err}} = \boldsymbol{K}_{\bar{\text{x}}}(\boldsymbol{R}_b)\bar{\boldsymbol{x}} + \boldsymbol{\xi} - \dot{\boldsymbol{x}}_{\text{ref}}$$

Asymptotic regulation of $\tilde{\boldsymbol{\xi}}(t)$ implies regulation of $\dot{\hat{\boldsymbol{x}}}_{\text{err}}(t) - \dot{\boldsymbol{x}}_{\text{err}}(t)$, and the former event is ensured by the properties of the observer established in Proposition 2, if boundedness of all the closed-loop signals can be established. This, indeed, will be proven in Proposition 5. The dynamics of $\dot{\hat{\boldsymbol{x}}}_{\text{err}}$ is governed by

$$\ddot{\hat{\boldsymbol{x}}}_{\text{err}} = \dot{\boldsymbol{K}}_{\bar{\text{x}}}(\boldsymbol{R}_b, \boldsymbol{\omega}_b)\bar{\boldsymbol{x}} + \boldsymbol{K}_{\bar{\text{x}}}(\boldsymbol{R}_b)\dot{\bar{\boldsymbol{x}}} + \dot{\boldsymbol{\xi}} - \ddot{\boldsymbol{x}}_{\text{ref}} \tag{31}$$

Solving for $\dot{\boldsymbol{\xi}}$ in the above identity and substituting the result in the equation of the observer dynamics (7), lead to the equation of the estimated augmented error dynamics in the form

$$\begin{aligned} \boldsymbol{M}(t,\hat{\boldsymbol{\theta}})\ddot{\hat{\boldsymbol{x}}}_{\text{err}} = &-\boldsymbol{C}(t,\hat{\boldsymbol{\theta}})\boldsymbol{\xi} + \boldsymbol{M}(t,\hat{\boldsymbol{\theta}})\big(\boldsymbol{K}_{\bar{\text{x}}}(\boldsymbol{R}_b)\dot{\bar{\boldsymbol{x}}} \\ &+ \dot{\boldsymbol{K}}_{\bar{\text{x}}}(\boldsymbol{R}_b, \boldsymbol{\omega}_b)\bar{\boldsymbol{x}} - \ddot{\boldsymbol{x}}_{\text{ref}}\big) - \boldsymbol{K}_{\text{o}}(t,\hat{\boldsymbol{\theta}})\tilde{\boldsymbol{\xi}} + \text{diag}(\hat{\boldsymbol{\lambda}})\boldsymbol{u} \end{aligned}$$

Let $\tilde{\boldsymbol{u}} := \boldsymbol{u} - \boldsymbol{u}^c$ be the mismatch between the actual forces and torques generated by the actuators and the ones commanded by the control system to the actuators. The control input

$$\begin{aligned} \text{diag}(\hat{\boldsymbol{\lambda}})\boldsymbol{u}^c := &\boldsymbol{C}(t,\hat{\boldsymbol{\theta}})\boldsymbol{\xi} - \boldsymbol{M}(t,\hat{\boldsymbol{\theta}})\big(\boldsymbol{K}_{\bar{\text{x}}}(\boldsymbol{R}_b)\dot{\bar{\boldsymbol{x}}} \\ &+ \dot{\boldsymbol{K}}_{\bar{\text{x}}}(\boldsymbol{R}_b, \boldsymbol{\omega}_b)\bar{\boldsymbol{x}} - \ddot{\boldsymbol{x}}_{\text{ref}}\big) - \boldsymbol{K}_{\text{o}}(t,\hat{\boldsymbol{\theta}})\dot{\boldsymbol{x}}_{\text{err}} \end{aligned} \tag{32}$$

yields the closed-loop dynamics

$$\boldsymbol{M}(\boldsymbol{q},\hat{\boldsymbol{\theta}})\ddot{\hat{\boldsymbol{x}}}_{\text{err}} = -\boldsymbol{K}_{\text{o}}(\boldsymbol{q},\hat{\boldsymbol{\theta}})\dot{\hat{\boldsymbol{x}}}_{\text{err}} - \text{diag}(\hat{\boldsymbol{\lambda}})\tilde{\boldsymbol{u}} \tag{33}$$

for the estimated augmented error.

**Proposition 4.** *Assume that $\boldsymbol{q}(t)$, $\hat{\boldsymbol{\theta}}(t)$, $\hat{\boldsymbol{\lambda}}(t)$ and $\tilde{\boldsymbol{u}}(t)$ exist for all $t \geq 0$. Then, the dynamics of the closed-loop system (33) is ISS with respect to the input $\tilde{\boldsymbol{u}}(\cdot)$, and satisfies the bounds*

$$\begin{aligned} ||\dot{\hat{\boldsymbol{x}}}_{\text{err}}(\cdot)||_\infty &\leq \max\left\{|\dot{\hat{\boldsymbol{x}}}_{\text{err}}(0)|, \frac{1}{k_o\, m_{\min}}||\tilde{\boldsymbol{u}}(\cdot)||_\infty\right\} \\ ||\dot{\hat{\boldsymbol{x}}}_{\text{err}}(\cdot)||_a &\leq \frac{1}{k_o\, m_{\min}}||\tilde{\boldsymbol{u}}(\cdot)||_a \end{aligned} \tag{34}$$

*where $m_{\min}$ is defined in (16).*

**Proof.** The result follows directly from Lemma 3.3 in Teel (1996) applied to the Lyapunov function $V_4(\dot{\hat{\boldsymbol{x}}}_{\text{err}}) = \frac{1}{2}\dot{\hat{\boldsymbol{x}}}_{\text{err}}^T\dot{\hat{\boldsymbol{x}}}_{\text{err}}$, and the fact that $\boldsymbol{M}(\boldsymbol{q},\hat{\boldsymbol{\theta}})$ satisfies (16) for all $\boldsymbol{q} \in \mathbb{R}^n$ and all $\hat{\boldsymbol{\theta}} \in \mathcal{M}_c^{n+1}$. More details are reported in Appendix B.

Proposition 4 establishes the robustness of the adaptive controller with respect to bounded mismatches between the actual and the commanded control input, that is, robustness to bounded input perturbations. Next, we present the main result that establishes boundedness of all trajectories and asymptotic regulation for vanishing input perturbations.

**Proposition 5.** *Assume that the signals $\boldsymbol{x}_{\text{ref}}(t)$, $\dot{\boldsymbol{x}}_{\text{ref}}(t)$, $\ddot{\boldsymbol{x}}_{\text{ref}}(t)$ and $\tilde{\boldsymbol{u}}(t)$, $t \geq 0$, are bounded. Then, all closed-loop trajectories exist for all $t \geq$*

0 *and are bounded. In addition, asymptotic regulation of the modified position/orientation error* $\bar{\boldsymbol{x}}(t)$ *is obtained for vanishing input disturbances* $\tilde{\boldsymbol{u}}(\cdot)$*, that is,*

$$||\tilde{\boldsymbol{u}}(\cdot)||_a = 0 \implies ||\bar{\boldsymbol{x}}(\cdot)||_a = 0 \tag{35}$$

**Proof.** Fix, arbitrarily, initial conditions for the closed-loop system, and let $[0, T_{\max})$, $T_{\max} \leq \infty$, denote the ensuing maximal interval of existence and uniqueness of solutions. From the proof of Proposition 4 found in Appendix B, the inequality

$$\dot{V}_4(\dot{\tilde{\boldsymbol{x}}}_{\text{err}}(t)) \leq -k_o |\dot{\tilde{\boldsymbol{x}}}_{\text{err}}(t)|^2 + m_{\min}^{-1} |\tilde{\boldsymbol{u}}(t)| \, |\dot{\tilde{\boldsymbol{x}}}_{\text{err}}(t)|$$

continues to hold for all $t \in [0, T_{\max})$. This, in turn, shows that $\dot{\tilde{\boldsymbol{x}}}_{\text{err}}(t)$ is bounded over $[0, T_{\max})$. As seen in the proof of Proposition 2, inequality (21) yields boundedness of the observation error $\tilde{\boldsymbol{\xi}}(t)$ over $[0, T_{\max})$. Since the estimated augmented error is defined as $\dot{\tilde{\boldsymbol{x}}}_{\text{err}} = \dot{\boldsymbol{x}}_{\text{err}} - \tilde{\boldsymbol{\xi}}$, the estimated augmented velocity error $\dot{\boldsymbol{x}}_{\text{err}}(t)$ is also bounded for all $t \in [0, T_{\max})$. Proposition 3 also holds for arbitrary truncation of the signals, thus there exists $\mu_{x_{\text{err}}} > 0$ such that $|\bar{\boldsymbol{x}}(t)| \leq \mu_{x_{\text{err}}}$ for all $t \in [0, T_{\max})$. Now, using Eqs. (26) and the previous bounds on $\bar{\boldsymbol{x}}(t)$ and $\dot{\boldsymbol{x}}_{\text{err}}(t)$, it follows that $\dot{\bar{\boldsymbol{x}}}(t)$ is bounded for all $t \in [0, T_{\max})$. Due to the definition of $\bar{\boldsymbol{x}}(t)$ and $\dot{\bar{\boldsymbol{x}}}(t)$, and since the reference trajectory is bounded for assumption, it follows that $\boldsymbol{q}(t)$ and $\dot{\boldsymbol{x}}(t)$ are bounded for all $t \in [0, T_{\max})$. Since both the observation error $\tilde{\boldsymbol{\xi}}(t)$ and the generalized velocities $\dot{\boldsymbol{x}}(t)$ are bounded, then the observed generalized velocities $\boldsymbol{\xi}(t)$ are also bounded for all $t \in [0, T_{\max})$. Using Eq. (32) and the results established so far, it follows that $\boldsymbol{u}^c(t)$ is bounded for all $t \in [0, T_{\max})$. Finally, considering Eq. (1), the definition of $\tilde{\boldsymbol{u}}(t)$ and using the bounds presented above, it follows that $\ddot{\boldsymbol{x}}(t)$ is bounded for all $t \in [0, T_{\max})$. Since we have proven that all signals in closed-loop are bounded over the maximal interval of existence and uniqueness, then $T_{\max} = \infty$.

Once it has been proven that all trajectories exist and are bounded over $[0, \infty)$, Proposition 2 yields asymptotic convergence of $\tilde{\boldsymbol{\xi}}(t)$. Due to the asymptotic bounds established in Proposition 4, if the input disturbances $\tilde{\boldsymbol{u}}(t)$ vanishes, the estimated augmented error $\dot{\tilde{\boldsymbol{x}}}_{\text{err}}(t)$ converges asymptotically. Owing to the definition of the augmented error, $\dot{\boldsymbol{x}}_{\text{err}} = \dot{\tilde{\boldsymbol{x}}}_{\text{err}} + \tilde{\boldsymbol{\xi}}$, it follows that $\dot{\boldsymbol{x}}_{\text{err}}(t)$ also converges to zero asymptotically. Finally, the modified position/orientation error $\bar{\boldsymbol{x}}(t)$ converges asymptotically as well, due to the asymptotic bounds (29) established in Proposition 3.

**Remark 1.** A few considerations are in order: First, Proposition 5 requires boundedness of the signal $\tilde{\boldsymbol{u}}(\cdot)$, meaning – in particular – that the references to be tracked must be commensurate to the available control authority in order to avoid continuously exceeding the overall physical limits of the system. Furthermore, the true benefits of the proposed solution are not immediately evident from the results provided in Propositions 2 through 5, as they relate to well-known anti-windup properties of indirect adaptive controller in the presence of input saturation, or, as dealt with in this paper, input mismatch – see Annaswamy and Wong (1997) and Karason and Annaswamy (1994). As a matter of fact, indirect or predictor-based solutions may exhibit a higher degree of robustness versus input disturbance than their direct counterpart, and this is indeed what emerges from the simulation study presented in the next section.

## 5. Simulation study

The effectiveness of the control solution proposed in this work is analyzed in simulation. The performance of the control scheme proposed in this study is compared to that of a modified version of the direct adaptive controller introduced in Wang and Xie (2009), which is inspired by the passivity-based controller outlined in Lee et al. (2018). The modifications are necessary as the straight adaptation of the controller of Wang and Xie (2009) to the free-flying scenario considered in this paper fails in the presence of loss of effectiveness of actuators. Specifically, the natural adaptive law from Lee et al. (2018) is incorporated into the controller of Wang and Xie (2009), together with the smooth projection operator defined in Krstic et al. (1995) to keep the estimated inertial parameters within the set of physically consistent parameters $\mathcal{M}_c^{n+1}$. The resulting controller can also be interpreted as a modification of the direct passivity-based adaptive controller of Lee et al. (2018) to encompass applications to space manipulator control. A challenging scenario is considered to test the robustness of the controller against model uncertainty, actuator wear, and unmodeled actuator nonlinearities.

**Table 3**
Characteristics of the chaser satellite.

| Mass [kg] | Position of COM [kg m] | Inertia ($\boldsymbol{I}_b$) [kg m$^2$] |
|---|---|---|
| $m_b = 1900$ | $\boldsymbol{p}_{bj} = \boldsymbol{0}$ | $I_{xx} = 13\,500$<br>$I_{yy} = 2000$<br>$I_{zz} = 14\,000$<br>$I_{ij} = 0$ |

**Table 4**
Denavit–Hartenberg parameters of the arm (Siciliano et al., 2008).

| | $l_1$ | $l_2$ | $l_3$ | $l_4$ | $l_5$ | $l_6$ | $l_7$ |
|---|---|---|---|---|---|---|---|
| $a_i$ [m] | 0 | 0 | 0 | 0 | 0 | 0 | 0 |
| $\alpha_i$ [rad] | $\pi/2$ | $-\pi/2$ | $\pi/2$ | $-\pi/2$ | $\pi/2$ | $-\pi/2$ | 0 |
| $d_i$ [m] | 0.3 | 0.16 | 1.15 | −0.16 | 1.15 | −0.16 | 0.4 |

**Table 5**
Characteristics of the grasped object.

| Parameters | Mass [kg] | Pos. COM [kg m] | Inertia [kg m$^2$] |
|---|---|---|---|
| Nominal | $m = 30$ | $h_c^x = 0$<br>$h_c^y = 0$<br>$h_c^z = 12$ | $I^{ii} = 40$<br>$I^{ij} = 0$ |
| True | $m = 100$ | $h_c^x = 0$<br>$h_c^y = 0$<br>$h_c^z = 40$ | $I_{xx} = 80$<br>$I^{yy} = 75$<br>$I^{zz} = 90$<br>$I^{ij} = 0$ |

### 5.1. Simulation setup

Simulations are performed on a realistic multibody model of the system built in Matlab/Simulink using the Mechanics toolbox, as similarly done in Pavanello et al. (2021). The characteristics of the SMS are inspired by actual space missions. The BS is represented as a box-shaped rigid body with two solar panels attached to its sides. The inertial parameters of the BS are listed in Table 3. The BS actuation system consists of a RCS and a group of four RWs whose dynamics are simulated in detail. The RCS is made up of 24 jet thrusters that can individually generate 10 [N] of thrust along the axis they are mounted on. Groups of four thrusters are mounted in the direction of the normal vector pointing outward with respect to each face of the BS cube-shaped body. The RWs together are able to generate 0.5 [Nm] of torque along each axis. The structure of the robotic arm is identical to the one described in Rank et al. (2011). The arm comprises seven links connected by revolute joints. The Denavit–Hartenberg parameters (see Siciliano et al. (2008)) of this configuration are listed in Table 4. The links are assumed to be hollow aluminum cylinders with a thickness of 13.5 [mm] and an external radius of 63.5 [mm]. The dynamics of the joints' motors are also included in the simulation model, where it is assumed that the motors can generate a maximum torque of 10 [Nm]. A white Gaussian noise with zero mean and variance of $\sigma = 10^{-7}$ is added to the measured position, attitude, and velocity signals to simulate sensor noise.

The gains of the two controllers are tuned to obtain comparable performance in nominal conditions in terms of energy consumption and

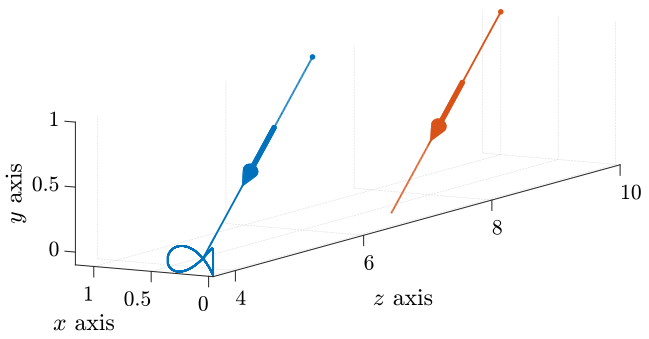


**Fig. 3.** Reference trajectory assigned to the EE represented in the inertial frame. The trajectories of the EE and BS are shown in blue and red, respectively. The initial positions of the BS and the EE are marked by two circles and the direction of motion of the BS and EE trajectories is indicated by two arrows. (For interpretation of the references to color in this figure legend, the reader is referred to the web version of this article.)

tracking error. The metric used to evaluate energy consumption is

$$E(\boldsymbol{v}(t)) = \int_0^{T_s} ||\boldsymbol{v}(s)||^2 ds$$

where $T_s$ is the length of the simulation and $\boldsymbol{v}(t)$ is a generic force or torque signal.

The trajectory followed by the space manipulator during the simulation can be divided into two parts. In the first one, i.e., within the interval $t \in [5, 35]$ [s], the BS moves diagonally while the position of arm joints is kept fixed, and then the whole system remains idle until $t = 70$ [s]. In the second one, between $t = 70$ [s] and $t = 170$ [s], an eight-shaped reference trajectory with a non-smooth velocity profile at its two ends is imposed on the EE while the pose of the BS remains fixed (see Fig. 3). During the entire trajectory, the orientation of both BS and EE are kept fixed. Even if the trajectory does not involve rotations, rotational dynamics are excited by the unknown grasped object. The average tracking error is defined as follows

$$A_v(\boldsymbol{e}(t)) = \frac{1}{T_s} \int_0^{T_s} ||\boldsymbol{e}(s)|| ds$$

where $\boldsymbol{e}(t)$ is a generic position or orientation error signal. In this setup, only the EE inertial parameters are considered to be uncertain. The a priori information on the grasped object inertial parameters is set to the values reported in Table 5.

### 5.2. Simulation results

Three scenarios are considered for comparison: the first one is used to establish a baseline in nominal conditions, in the second one the effectiveness of two motors of the robotic arm is compromised during the simulation, and in the final one in addition to the efficiency loss also the dynamics of the actuators are simulated.

In the first scenario, the dynamics of the actuators are not included in the simulation model. Hence, the control wrenches are directly applied to the rigid bodies of the space manipulator system. As mentioned, the two controllers are tuned to perform similarly in terms of energy consumption, as confirmed by the data reported in Table 6. The Euclidean norm of tracking error of the EE position, denoted as $\tilde{\boldsymbol{p}}_e^i := \boldsymbol{p}_e^i - \boldsymbol{p}_{e,\text{ref}}^i \in \mathbb{R}^3$, and the metric

$$d_F(\tilde{\boldsymbol{R}}_e) := \sqrt{\frac{1}{2}||\tilde{\boldsymbol{R}}_e - \mathbb{I}_{3\times3}||_F^2}$$

representing the chordal distance between $\tilde{\boldsymbol{R}}_e := \boldsymbol{R}_{e,\text{ref}}^T \boldsymbol{R}_e \in SO(3)$ and the identity matrix, offer a practical way to measure the cumulative impact of tracking errors stemming from both the BS and the arm joints. Therefore, these errors are utilized to depict the tracking error

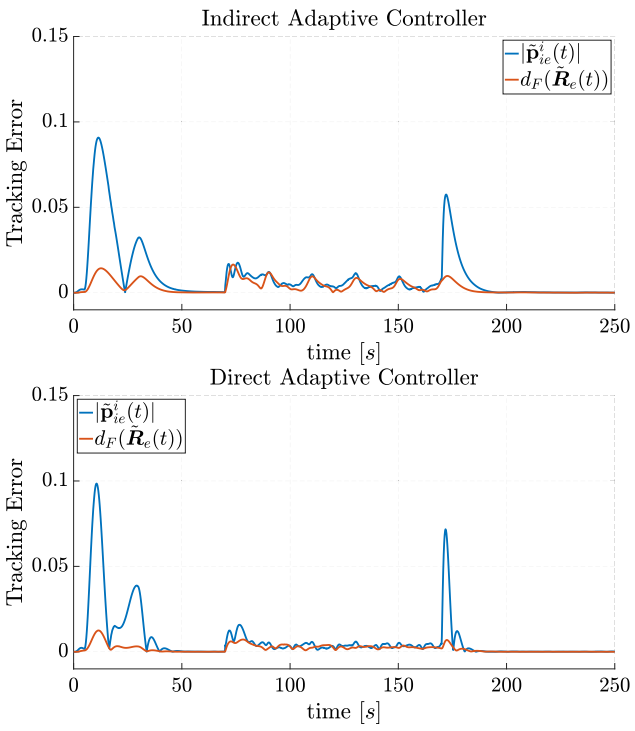


**Fig. 4.** Scenario 1. Time history of the position and orientation errors of the EE.

**Table 6**
Controllers performance – Scenario 1.

| | Indirect | Direct |
|---|---|---|
| Position error BS [m] | $0.453 \times 10^{-3}$ | $0.352 \times 10^{-3}$ |
| Orientation error BS | $0.16 \times 10^{-3}$ | $0.0423 \times 10^{-3}$ |
| Position error EE [m] | $9.41 \times 10^{-3}$ | $6.96 \times 10^{-3}$ |
| Orientation error EE | $1.68 \times 10^{-3}$ | $0.942 \times 10^{-3}$ |
| Energy of RCS force [$N^2$ s] | 51 060 | 59 046 |
| Energy of RCS torque [$N^2$ $m^2$ s] | 25 276 | 21 561 |
| Energy of RW torque [$N^2$ $m^2$ s] | 172.31 | 167.51 |
| Energy of joints torque [$N^2$ $m^2$ s] | 3610.4 | 3816.9 |

**Table 7**
Controllers performance – Scenario 2.

| | Indirect | Direct |
|---|---|---|
| Position error BS [m] | $0.673 \times 10^{-3}$ | $0.352 \times 10^{-3}$ |
| Orientation error BS | $0.21 \times 10^{-3}$ | $0.0423 \times 10^{-3}$ |
| Position error EE [m] | $11.1 \times 10^{-3}$ | $20.9 \times 10^{-3}$ |
| Orientation error EE | $2.43 \times 10^{-3}$ | $8.05 \times 10^{-3}$ |
| Energy of RCS force [$N^2$ s] | 51 264 | 60 387 |
| Energy of RCS torque [$N^2$ $m^2$ s] | 26 212 | 28 377 |
| Energy of RW torque [$N^2$ $m^2$ s] | 172.33 | 168.45 |
| Energy of joints torque [$N^2$ $m^2$ s] | 6046.4 | 10 133 |

in graphical representations. Similar closed-loop performance in terms of the tracking errors are obtained, as seen in Fig. 4 and from the data in Table 6, where the average errors are reported. The time history of the estimation error of the inertia parameters is reported in Fig. 5. The first two peaks of the tracking error in Fig. 4 are associated with the initial adaptation of the inertia parameters, while the second phase of adaptation corresponds to the eight-shaped part of the trajectory where the tracking error is again different than zero. Notice that as soon as the tracking error becomes sufficiently small, the adaptation resumes when the system dynamics are again excited by the reference trajectory. The peak in the tracking occurring around $t = 170$ [s] is due to a non-smooth change in velocity reference.

The second scenario concerns the analysis of the effect of a partial failure of the actuation system occurring at $t = 120$ [s]. In particular, the

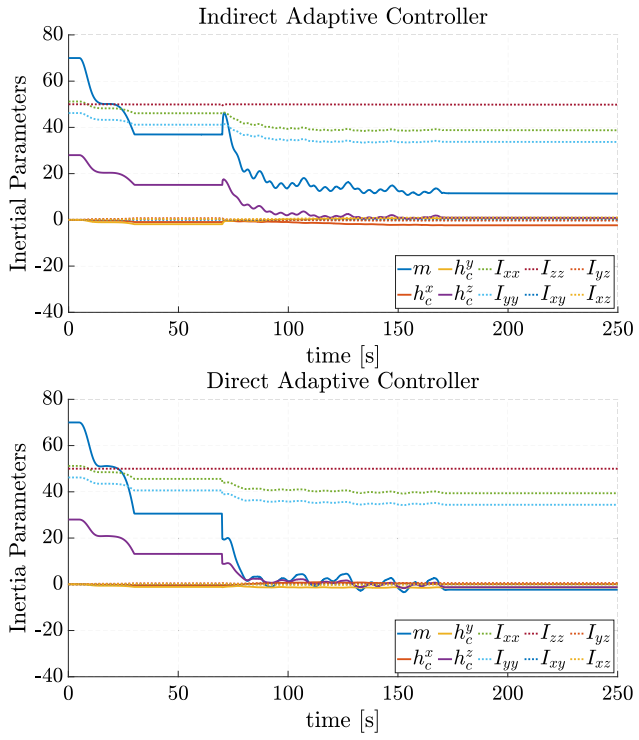


**Fig. 5.** Scenario 1. Time history of the estimation error of the inertial parameters.

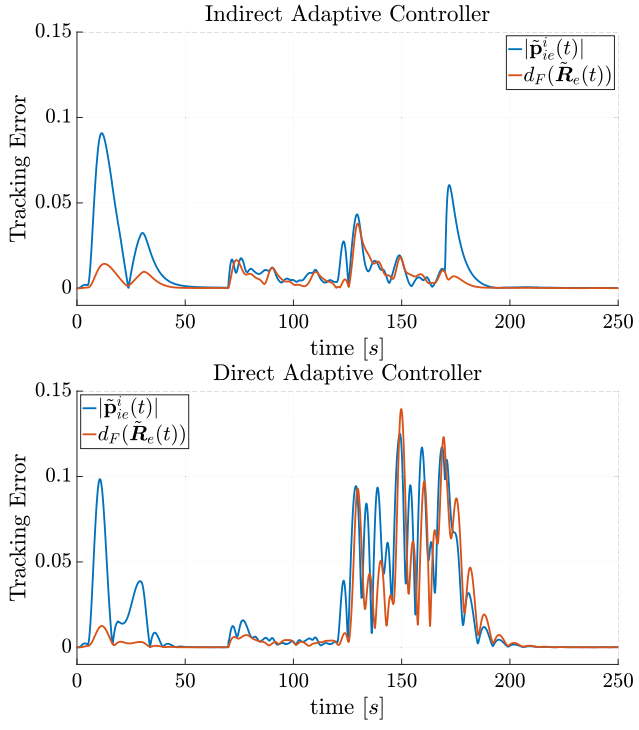


**Fig. 6.** Scenario 2. Time history of the position and orientation errors of the EE.

efficiency of joints 1 and 4 is reduced to 60% and 50 % of their nominal values, respectively. The time histories of the EE tracking error and the inertial parameters estimates are shown in Figs. 6 and 7, respectively. A strong similarity with the results of the first scenario is noticed until the $t = 120$ [s] time mark. After that, the performance of the direct adaptive controller worsens significantly as a consequence of the loss of efficiency, as confirmed by the data in Table 7. The performance

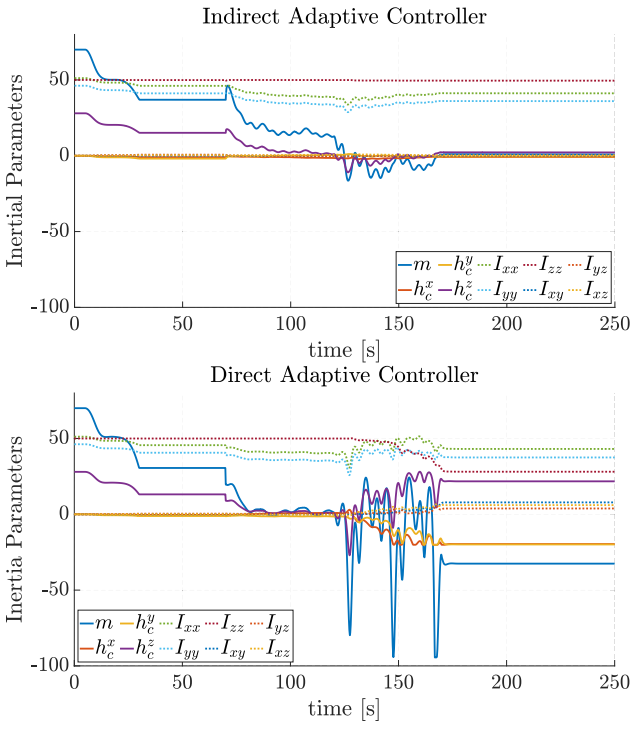


**Fig. 7.** Scenario 2. Time history of the estimation error of the inertial parameters.

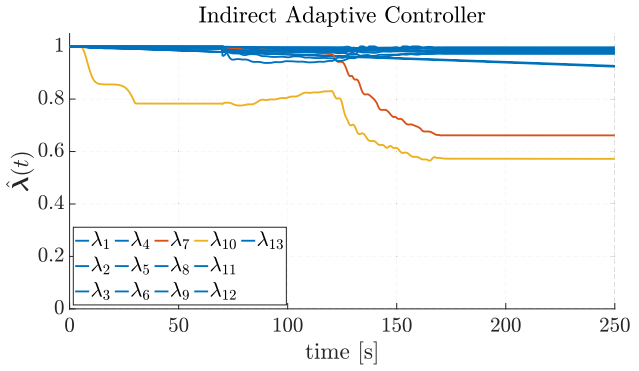


**Fig. 8.** Scenario 2. Estimated actuators' efficiencies. The two joints whose efficiency is reduced at $t = 120$ [s] are displayed in red and yellow, the others in blue. (For interpretation of the references to color in this figure legend, the reader is referred to the web version of this article.)

deterioration is a consequence of the drift of the inertial parameter estimates, as the direct controller reacts abnormally to the efficiency loss by re-tuning the inertial parameters (this is clearly noticeable from Fig. 7). Conversely, the results provided by the indirect controller show a transient behavior in the parameter estimation error, which converges to a constant. The change in actuator efficiency is compensated by the adaptation of the parameters $\lambda_7$ and $\lambda_{10}$, as seen in Fig. 8, showing the time history of the estimates $\hat{\lambda}(t)$. Examination of Fig. 9, which shows the time history of the eigenvalues of $f(\hat{\theta})$ of the direct adaptive controller, confirms that across the second simulation scenario, in spite of a noticeable drift, the estimated inertial parameters of the EE are always physically consistent.

In the final simulation scenario, the dynamics of the actuators are included in the simulation model. The combined effect of un-modeled nonlinearities and input saturation leads to the direct controller failing. Due to the configuration of the jet-thrusters on the BS, a maximum of 40 [N] of force can be applied along each principal axis of the

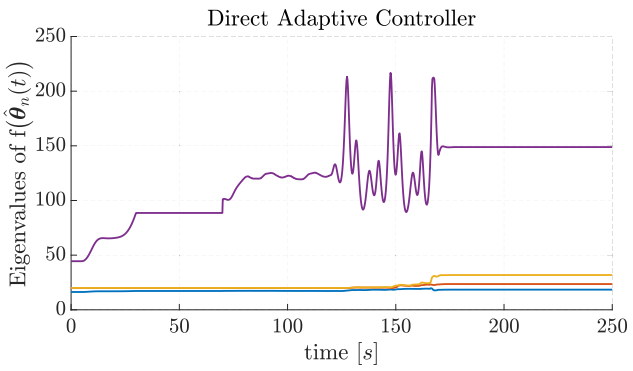


**Fig. 9.** Scenario 2. Eigenvalues of the direct adaptive controller estimated inertial parameters of the combined grasped object and EE, mapped on $\mathcal{P}(4)$.

**Table 8**
Controller performance scenario 3.

| | Indirect Controller |
|---|---|
| Position error BS [m] | $27.6 \times 10^{-3}$ |
| Orientation error BS | $0.308 \times 10^{-3}$ |
| Position error EE [m] | $23.5 \times 10^{-3}$ |
| Orientation error EE | $3.45 \times 10^{-3}$ |
| Energy of RCS force [N$^2$ s] | 65 870 |
| Energy of RCS torque [N$^2$ m$^2$ s] | 109 880 |
| Energy of RW torque [N$^2$ m$^2$ s] | 97.022 |
| Energy of torque at joints [N$^2$ m$^2$ s] | 5358.9 |

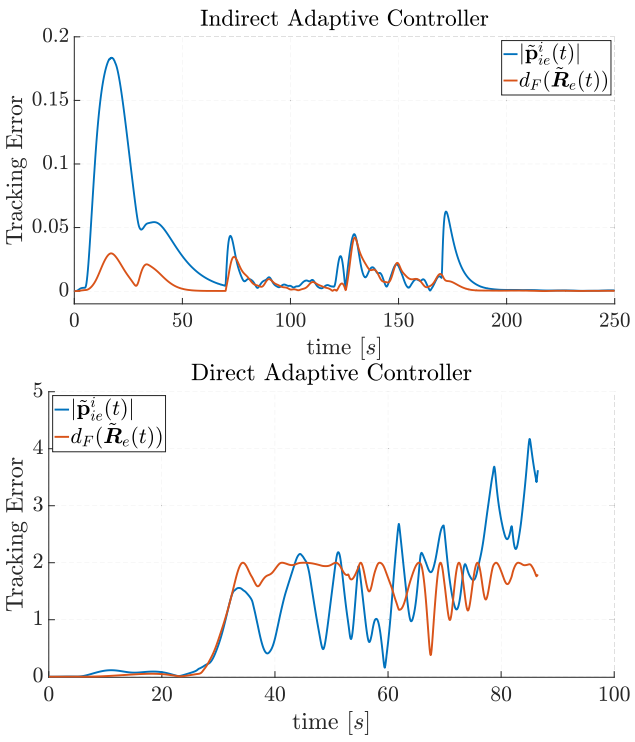


**Fig. 10.** Scenario 3. Time history of the position and orientation errors of the EE.

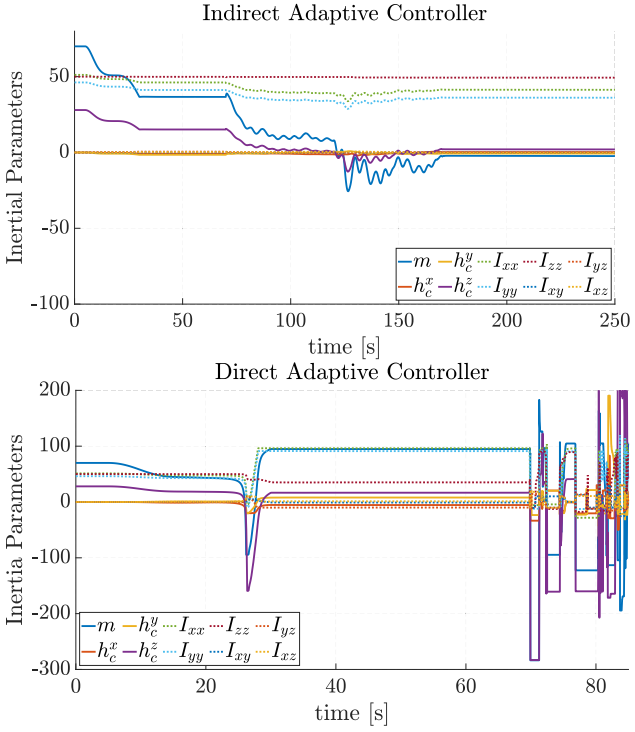


**Fig. 11.** Scenario 3. Time history of the estimation error of the inertial parameters.

body (i.e., the axes of the $\mathcal{B}$ frame). However, this value represents only an upper bound; if torques are also required to be applied on the BS body frame, this value is not fully available for force production since the same thrusters are used to generate torque. Fig. 12 shows the resultant of the forces assigned by the direct adaptive controller and the one actually produced by the actuators, where the saturation of the actuators is clearly noticeable. For comparison, the same two quantities as provided by the indirect controller are shown in Fig. 13.

Due to the occurrence of input saturation, the inertia parameter estimates of the direct controller drift, and approach the boundary of the parameter set $\mathcal{M}_c$ at around $t = 26$ [s] (see Fig. 11). From this time on, the direct controller loses authority, as apparent from the pose error of the EE shown in Fig. 10. On the other hand, the indirect control solution proposed in this work behaves similarly to the second scenario in spite of actuator saturation, as can be noticed by comparing Fig. 10 with Fig. 6, and Fig. 11 with Fig. 7. The larger values reported in table are due to an initial position error of the BS that can be associated with the actuator saturation. As a matter of fact, it can be noticed from Fig. 10 that, when nominal conditions are restored, the EE pose error assumes values comparable to the ones obtained in the second case study (see Table 8).

## 6. Conclusions

In this work, an indirect adaptive solution has been proposed to control a SMS in the presence of uncertainties and input disturbances. First, an observer for the generalized velocities of the system is designed with the purpose of estimating online a set of parameters that capture the stimulated system dynamics. Then, a controller is designed on the basis of the adaptive observer serving as a proxy of the actual system dynamics. The performance of both the observer and controller is analyzed. Finally, a high-fidelity simulation environment, where realistic dynamics of both the system and the actuators are modeled, is employed to test closed-loop performance. A partially known grasped object is moved along a non-smooth trajectory during which an efficiency loss of the actuators is simulated.

The proposed controller has shown in simulation to achieve improved closed-loop performance in comparison with state-of-the-art solutions when the effect of actuator non-idealities is considered. This

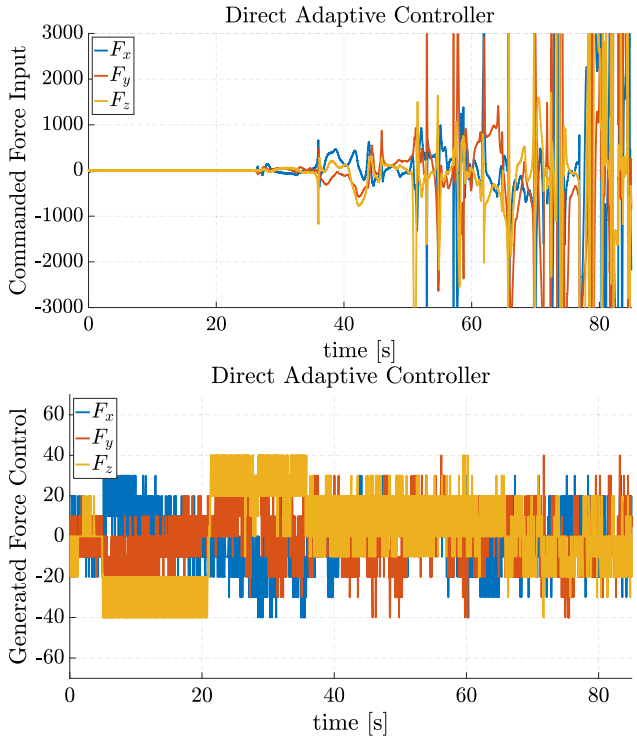


**Fig. 12.** Scenario 3. Time history of the direct controller commanded force control and the generated force control by the RCS, both expressed in the frame $\mathcal{B}$ coordinates.

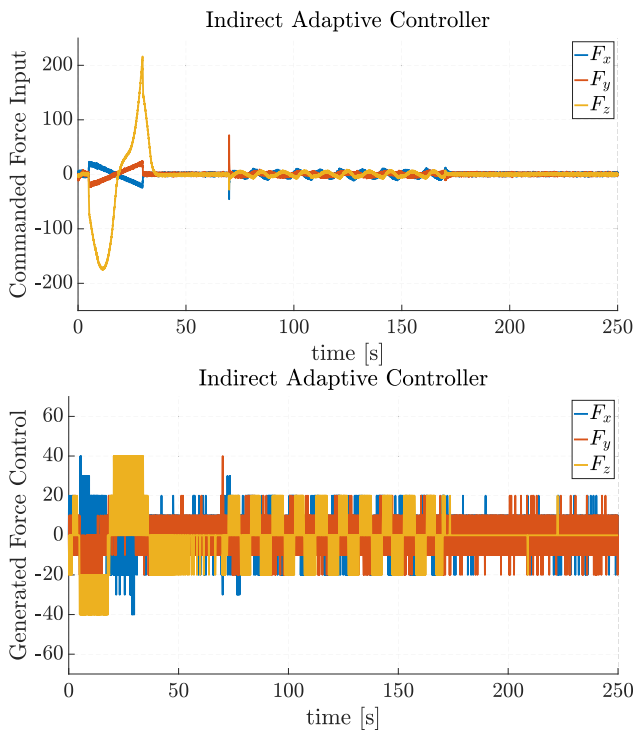


**Fig. 13.** Scenario 3. Time history of the indirect controller commanded force control and the generated force control by the RCS, both expressed in the frame $\mathcal{B}$ coordinates.

capability stems from the fact that in our indirect adaptive controller the regressor depends directly on the *actual* control signal, hence the adaptation mechanism does not react abnormally to mismatches between the signal computed by the controller and the action produced by the actuator. This property of indirect scheme has been observed in the literature for linear systems since the early work of Annaswamy and Wong (1997) and Karason and Annaswamy (1994). We believe – to the best of our knowledge – that this feature has been used in the context of control of robotics systems for the first time in this work.

## CRediT authorship contribution statement

**Jacopo Giordano:** Writing – original draft, Validation, Software, Methodology, Investigation, Formal analysis, Data curation, Conceptualization. **Angelo Cenedese:** Writing – review & editing, Supervision, Resources, Project administration, Methodology, Funding acquisition, Conceptualization. **Andrea Serrani:** Writing – review & editing, Supervision, Methodology, Formal analysis.

## Declaration of competing interest

The authors declare the following financial interests/personal relationships which may be considered as potential competing interests: Jacopo Giordano reports financial support was provided by Ministero dell'Università e della Ricerca and Gini Foundation. Jacopo Giordano reports a relationship with Ministero dell'università e della ricerca and Gini Foundation that includes: funding grants. None If there are other authors, they declare that they have no known competing financial interests or personal relationships that could have appeared to influence the work reported in this paper.

## Appendix A. Lyapunov function for the inertial parameters

The Lyapunov function proposed in Lee et al. (2018) and employed in this work for the inertial parameters of the space manipulator is reported here for completeness alongside the calculations necessary to find its Lie derivative. Consider

$$V_p = \sum_{j=0}^{n} \gamma_{\theta_j}^{-1} D_{F(\mathcal{P}(4))}(f(\hat{\theta}_j)||f(\theta_j)) = \sum_{j=0}^{n} \gamma_{\theta_j}^{-1} \sum_{k=0}^{4} \left[-\log(\lambda_j^k) + \lambda_j^k - 1\right] \tag{A.1}$$

where $\lambda_j^k$, $k = 1, \dots, 4$ are the eigenvalues of $f(\hat{\theta}_j)^{-1} f(\theta_j)$ and $\gamma_{\theta_j}^{-1}$ is a scalar positive gain. The function (A.1) is a valid Lyapunov candidate function since $-\log(x) + x - 1$ is positive definite and proper on $(0, \infty)$, and vanishes at $x = 1$. Note that the pseudo distance (6) is not defined for physically inconsistent values of the parameters of the rigid body, and diverges as the parameters approach the boundary of the feasible set. The Lie derivative of (A.1) is

$$\begin{aligned}
\dot{V}_p &= \frac{d}{dt} \sum_{j=0}^{n} \gamma_{\theta_j}^{-1} \left[ \log\left( \frac{\det\left(f(\hat{\theta}_j)\right)}{\det\left(f(\theta_j)\right)} \right) + \operatorname{tr}\left(f(\hat{\theta}_j)^{-1} f(\theta_j)\right) - 4 \right] \\
&= \sum_{j=0}^{n} \gamma_{\theta_j}^{-1} \operatorname{tr}\left( f(\hat{\theta}_j)^{-1} f(\dot{\hat{\theta}}_j) - f(\hat{\theta}_j)^{-1} f(\dot{\hat{\theta}}_j) f(\hat{\theta}_j)^{-1} f(\theta_j) \right) \\
&= \sum_{j=0}^{n} \gamma_{\theta_j}^{-1} \operatorname{tr}\left( f(\hat{\theta}_j)^{-1} f(\dot{\hat{\theta}}_j) f(\hat{\theta}_j)^{-1} \left( f(\hat{\theta}_j) - f(\theta_j) \right) \right) \\
&= -\sum_{j=0}^{n} \gamma_{\theta_j}^{-1} \operatorname{tr}\left( f(\hat{\theta}_j)^{-1} f(\dot{\hat{\theta}}_j) f(\hat{\theta}_j)^{-1} f(\tilde{\theta}_j) \right)
\end{aligned} \tag{A.2}$$

where the linearity of the mapping (4) and the identities

$$\frac{d}{dt}\left(\log\left(\det(\boldsymbol{X})\right)\right) = \operatorname{tr}\left(\boldsymbol{X}^{-1} \frac{d\boldsymbol{X}}{dt}\right) =$$

$$\frac{d\boldsymbol{X}^{-1}}{dt} = -\boldsymbol{X}^{-1} \frac{d\boldsymbol{X}}{dt} \boldsymbol{X}^{-1}$$

are used. Eq. (A.2) can be rewritten as follows owing to the identity (9)

$$\dot{V}_p = -\sum_{j=0}^{n} \gamma_{\theta_j}^{-1} \dot{\hat{\theta}}_j^T g(\hat{\theta}_j) \tilde{\theta}_j$$

## Appendix B

*Proof of Proposition 3*

It will be shown that $V_1(\tilde{\boldsymbol{p}}_b^i) = \frac{1}{2}\left(\tilde{\boldsymbol{p}}_b^i\right)^T \tilde{\boldsymbol{p}}_b^i$, $V_2(\tilde{\boldsymbol{\sigma}}) = 2\ln(1+\tilde{\boldsymbol{\sigma}}^T\tilde{\boldsymbol{\sigma}})$, and $V_3(\tilde{\boldsymbol{q}}) = \frac{1}{2}\tilde{\boldsymbol{q}}^T\tilde{\boldsymbol{q}}$ are ISS-Lyapunov functions for the dynamics of the modified position/orientation error $\tilde{\boldsymbol{x}}$. The Lie derivative of $V_1(\tilde{\boldsymbol{p}})$ satisfies

$$\begin{aligned}\dot{V}_1(\tilde{\boldsymbol{p}}) &= -\left(\tilde{\boldsymbol{p}}_b^i\right)^T \tilde{\boldsymbol{p}}_b^i = -\left(\tilde{\boldsymbol{p}}_b^i\right)^T \boldsymbol{K}_{\mathrm{p}} \tilde{\boldsymbol{p}}_b^i + \left(\tilde{\boldsymbol{p}}_b^i\right)^T \boldsymbol{R}_b \boldsymbol{\nu}_{\mathrm{err}} \\ &\leq -\lambda_{\min}(\boldsymbol{K}_{\mathrm{p}})|\tilde{\boldsymbol{p}}_b^i|^2 + \lambda_{\max}(\boldsymbol{R}_b)|\tilde{\boldsymbol{p}}_b^i||\boldsymbol{\nu}_{\mathrm{err}}| \\ &\leq -|\tilde{\boldsymbol{p}}_b^i|\left[\lambda_{\min}(\boldsymbol{K}_{\mathrm{p}})|\tilde{\boldsymbol{p}}_b^i| - |\boldsymbol{\nu}_{\mathrm{err}}|\right]\end{aligned}$$

Clearly,

$$|\tilde{\boldsymbol{p}}_b^i| > \frac{1}{\lambda_{\min}(\boldsymbol{K}_{\mathrm{p}})}|\boldsymbol{\nu}_{\mathrm{err}}| \Rightarrow \dot{V}_1(\tilde{\boldsymbol{p}}_b^i) < 0$$

where $\lambda_{\min}(\cdot)$ and $\lambda_{\max}(\cdot)$ denote the minimum and maximum eigenvalue of the argument matrix, respectively. The Lie derivative of $V_2(\tilde{\boldsymbol{\sigma}})$ is computed as follows

$$\dot{V}_2(\tilde{\boldsymbol{\sigma}}) = \frac{\partial V_2(\tilde{\boldsymbol{\sigma}})}{\partial \tilde{\boldsymbol{\sigma}}}\dot{\tilde{\boldsymbol{\sigma}}} = \tilde{\boldsymbol{\sigma}}^T\tilde{\boldsymbol{\omega}} = -\tilde{\boldsymbol{\sigma}}^T\left[\boldsymbol{K}_\sigma\tilde{\boldsymbol{\sigma}} - \boldsymbol{\omega}_{\mathrm{err}}\right]$$

and satisfies

$$\dot{V}_2(\tilde{\boldsymbol{\sigma}}) \leq -|\tilde{\boldsymbol{\sigma}}|\left[\lambda_{\min}(\boldsymbol{K}_\sigma)|\tilde{\boldsymbol{\sigma}}| - |\boldsymbol{\omega}_{\mathrm{err}}|\right]$$

similarly to the previous case, one obtains

$$|\tilde{\boldsymbol{\sigma}}| > \frac{1}{\lambda_{\min}(\boldsymbol{K}_\sigma)}|\boldsymbol{\omega}_{\mathrm{err}}| \Rightarrow \dot{V}_2(\tilde{\boldsymbol{\sigma}}) < 0$$

Using a similar procedure, the following relationship is obtained for the Lie derivative of $V_3(\tilde{\boldsymbol{q}})$:

$$|\tilde{\boldsymbol{q}}| > \frac{1}{\lambda_{\min}(\boldsymbol{K}_{\mathrm{q}})}|\boldsymbol{q}_{\mathrm{err}}| \Rightarrow \dot{V}_3(\tilde{\boldsymbol{q}}) < 0$$

As a consequence, $V_1$, $V_2$ and $V_3$ are ISS-Lyapunov function (Teel, 1996, Lemma 3.3). The bounds (28),(29) and (34) follow from the results in Teel (1996) as well.

*Proof of Proposition 4*

Since by assumption the matrix-valued function $\boldsymbol{M}(\boldsymbol{q}(t), \hat{\boldsymbol{\theta}}(t))$ exists and is (uniformly) positive definite for all $t \geq 0$, system (33) can be equivalently written as

$$\ddot{\tilde{\boldsymbol{x}}}_{\mathrm{err}} = -k_o\dot{\tilde{\boldsymbol{x}}}_{\mathrm{err}} + \boldsymbol{M}(\boldsymbol{q}(t), \hat{\boldsymbol{\theta}}(t))^{-1}\mathrm{diag}(\hat{\boldsymbol{\lambda}}(t))\tilde{\boldsymbol{u}}(t)$$

which takes the form of an internally stable LTI system driven by a external disturbance. The Lie derivative of the Lyapunov function candidate $V_4(\dot{\tilde{\boldsymbol{x}}}_{\mathrm{err}}) = \frac{1}{2}\dot{\tilde{\boldsymbol{x}}}_{\mathrm{err}}^T\dot{\tilde{\boldsymbol{x}}}_{\mathrm{err}}$ satisfies

$$\begin{aligned}\dot{V}_4(\dot{\tilde{\boldsymbol{x}}}_{\mathrm{err}}) &\leq -k_o|\dot{\tilde{\boldsymbol{x}}}_{\mathrm{err}}|^2 + ||\boldsymbol{M}(\boldsymbol{q}, \hat{\boldsymbol{\theta}})^{-1}||\,||\mathrm{diag}(\hat{\boldsymbol{\lambda}})||\,|\tilde{\boldsymbol{u}}|\,|\dot{\tilde{\boldsymbol{x}}}_{\mathrm{err}}| \\ &\leq -k_o|\dot{\tilde{\boldsymbol{x}}}_{\mathrm{err}}|^2 + m_{\min}^{-1}|\tilde{\boldsymbol{u}}|\,|\dot{\tilde{\boldsymbol{x}}}_{\mathrm{err}}|\end{aligned}$$

Consequently,

$$|\dot{\tilde{\boldsymbol{x}}}_{\mathrm{err}}| > \frac{1}{k_o\, m_{\min}}|\tilde{\boldsymbol{u}}| \Rightarrow \dot{V}_4(\dot{\tilde{\boldsymbol{x}}}_{\mathrm{err}}) < 0$$

showing that $V_4(\dot{\tilde{\boldsymbol{x}}}_{\mathrm{err}})$ is an ISS-Lyapunov function for (33). The bounds then follow from Lemma 3.3 in Teel (1996).

## References


Abiko, S., & Hirzinger, G. (2009). Adaptive control for a torque controlled free-floating space robot with kinematic and dynamic model uncertainty. In *2009 IEEE/RSJ international conference on intelligent robots and systems* (pp. 2359–2364). IEEE.

Annaswamy, A., & Wong, J. (1997). Adaptive control in the presence of saturation non-linearity. *International Journal of Adaptive Control and Signal Processing*, *11*, 3–19.

Bonnal, C., Ruault, J., & Desjean, M. (2013). Active debris removal: Recent progress and current trends. *Acta Astronautica*, *85*, 51–60.

Christidi-Loumpasefski, O., Rekleitis, G., & Papadopoulos, E. (2020). Concurrent parameter identification and control for free-floating robotic systems during on-orbit servicing. In *2020 IEEE international conference on robotics and automation* (pp. 6014–6020). IEEE.

Dou, B., & Yue, X. (2023). Disturbance observer-based fractional-order sliding mode control for free-floating space manipulator with disturbance. *Aerospace Science and Technology*, *132*, Article 108061.

Flores-Abad, A., Ma, O., Pham, K., & Ulrich, S. (2014). A review of space robotics technologies for on-orbit servicing. *Progress in Aerospace Sciences*, *68*, 1–26.

Giordano, J., Cenedese, A., & Serrani, A. (2024). A natural indirect adaptive controller for a satellite-mounted manipulator. In *2024 American control conference*. ACC, Toronto, CA.

Giordano, A., Ott, C., & Albu-Schäffer, A. (2019). Coordinated control of spacecraft's attitude and end-effector for space robots. *IEEE Robotics and Automation Letters*, *4*, 2108–2115.

Ioannou, P., & Sun, J. (1996). *Robust adaptive control*. Prentice Hall Englewood Cliffs, NJ.

Jia, S., & Shan, J. (2019). Finite-time trajectory tracking control of space manipulator under actuator saturation. *IEEE Transactions on Industrial Electronics*, *67*, 2086–2096.

Karason, S., & Annaswamy, A. (1994). Adaptive control in the presence of input constraints. *IEEE Transactions on Automatic Control*, *39*, 2325–2330.

Krstic, M., Kokotovic, P., & Kanellakopoulos, I. (1995). *Nonlinear and adaptive control design*. John Wiley & Sons, Inc.

Lee, T., Kwon, J., & Park, F. (2018). A natural adaptive control law for robot manipulators. In *2018 IEEE/RSJ international conference on intelligent robots and systems* IROS, (pp. 1–9). IEEE.

Lee, T., & Park, F. (2018). A geometric algorithm for robust multibody inertial parameter identification. *IEEE Robotics and Automation Letters*, *3*, 2455–2462.

Nicolis, D., Allevi, F., & Rocco, P. (2020). Operational space model predictive sliding mode control for redundant manipulators. *IEEE Transactions on Robotics*, *36*, 1348–1355.

Papadopoulos, E., Aghili, F., Ma, O., & Lampariello, R. (2021). Robotic manipulation and capture in space: A survey. *Frontiers in Robotics and AI*, *228*.

Parlaktuna, O., & Ozkan, M. (2004). Adaptive control of free-floating space manipulators using dynamically equivalent manipulator model. *Robotics and Autonomous Systems*, *46*, 185–193.

Pavanello, Z., Branz, F., Francesconi, A., Cenedese, A., Antonello, R., Basana, F., Iob, P., Vertuani, D., Massari, M., & Colombo, C. (2021). Combined control and navigation approach to the robotic capture of space vehicles. In *International astronautical congress* ICA, (pp. 1–13).

Rank, P., Mühlbauer, Q., Naumann, W., & Landzettel, K. (2011). The DEOS automation and robotics payload. In *Symp. on advanced space technologies in robotics and automation*. the Netherlands: ASTRA.

Rognant, M., Cumer, C., Biannic, J., Roa, M., Verhaeghe, A., & Bissonnette, V. (2019). Autonomous assembly of large structures in space: a technology review. In *European conf. for aeronautics and aerospace sciences*. EUCASS.

Seddaoui, A., & Saaj, C. (2019). Combined nonlinear h-infitiy controller for a controlled-floating space robot. *Journal of Guidance, Control, and Dynamics*, *42*, 1878–1885.

Shao, X., Sun, G., Xue, C., & Li, X. (2021). Nonsingular terminal sliding mode control for free-floating space manipulator with disturbance. *Acta Astronautica*, *181*, 396–404.

Siciliano, B., Sciavicco, L., Villani, L., & Oriolo, G. (2008). *Robotics: modelling, planning and control* (1st ed.). Springer Publishing Company, Incorporated.

Sontag, E. (2008). Input to state stability: Basic concepts and results. In P. Nistri, & G. Stefani (Eds.), *Lecture notes in mathematics: vol. 1932, Nonlinear and optimal control theory* (pp. 163–220). Springer Verlag.

Spong, M., Hutchinson, S., & Vidyasagar, M. (2020). *Robot modeling and control*. John Wiley & Sons.

Teel, A. (1996). A nonlinear small gain theorem for the analysis of control systems with saturation. *IEEE Transactions on Automatic Control*, *41*, 1256–1270.

Tsiotras, P. (1996). Stabilization and optimality results for the attitude control problem. *Journal of Guidance, Control, and Dynamics*, *19*, 772–779.

Wang, H., & Xie, Y. (2009). Passivity based adaptive jacobian tracking for free-floating space manipulators without using spacecraft acceleration. *Automatica*, *45*, 1510–1517.

Wang, H., & Xie, Y. (2012). Prediction error based adaptive jacobian tracking for free-floating space manipulators. *IEEE Transactions on Aerospace and Electronic Systems*, *48*, 3207–3221.

Wensing, P., Kim, S., & Slotine, J. (2017). Linear matrix inequalities for physically consistent inertial parameter identification: A statistical perspective on the mass distribution. *IEEE Robotics and Automation Letters*, *3*, 60–67.

Yao, Q. (2021). Adaptive trajectory tracking control of a free-flying space manipulator with guaranteed prescribed performance and actuator saturation. *Acta Astronautica*, *185*, 283–298.

Zhao, J., Jiang, S., Xie, F., Wang, X., & Li, Z. (2019). Adaptive dynamic sliding mode control for space manipulator with external disturbance. *Journal of Control and Decision*, *6*, 236–251.